Cell Reports
Methods

Article

Transgenic sensors reveal compartment-specific effects of aggregation-prone proteins on subcellular proteostasis during aging

Graphical abstract

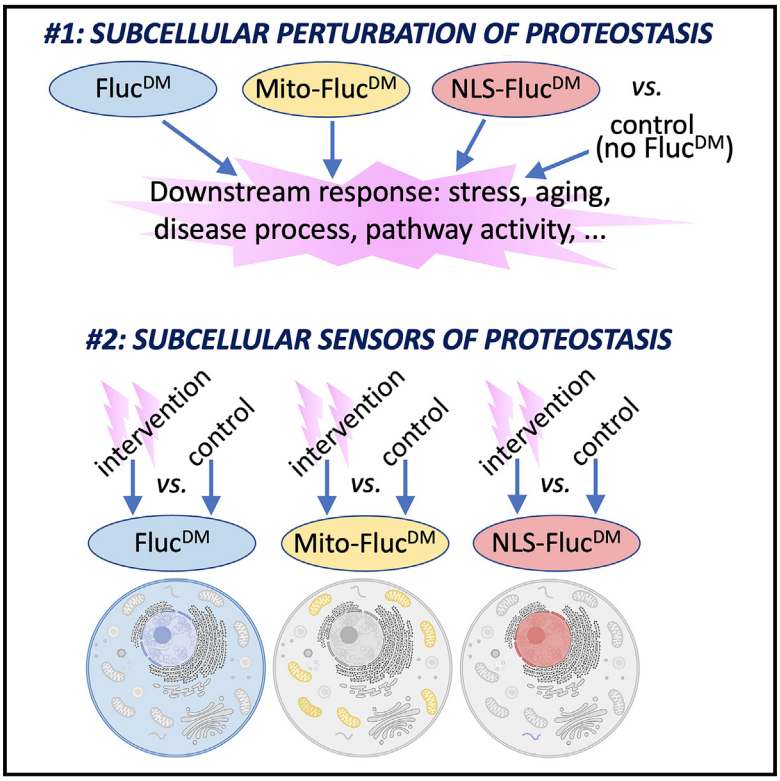

Highlights

- Establishes transgenic sensors of subcellular proteostasis in *Drosophila*
- Demonstrates their use to monitor proteostasis in different cell compartments
- Examines how inter-organ signaling impacts subcellular proteostasis
- Shows that pathogenic tau^{V337M} differentially remodels proteome solubility

Authors

Michelle Curley, Mamta Rai, Chia-Lung Chuang, ..., Yong-Dong Wang, Junmin Peng, Fabio Demontis

Correspondence

fabio.demontis@stjude.org

In brief

Curley et al. develop transgenic sensors of subcellular proteostasis in *Drosophila* based on misfolding-prone Fluc^{DM} protein variants that localize to the cytoplasm, nucleus, and mitochondria. They demonstrate that these tools can be used to monitor how cellular stress, inter-organ signaling, and aggregation-prone proteins impact subcellular proteostasis during aging in *Drosophila*.

Curley et al., 2024, Cell Reports Methods *4*, 100875
October 21, 2024
https://doi.org/10.1016/j.crmeth.2024.100875

CellPress

Cell Reports Methods

CellPress
OPEN ACCESS

Article

Transgenic sensors reveal compartment-specific effects of aggregation-prone proteins on subcellular proteostasis during aging

Michelle Curley,[1] Mamta Rai,[1] Chia-Lung Chuang,[1] Vishwajeeth Pagala,[2] Anna Stephan,[1] Zane Coleman,[1] Maricela Robles-Murguia,[1] Yong-Dong Wang,[3] Junmin Peng,[1,2,4] and Fabio Demontis[1,5,*]

[1]Department of Developmental Neurobiology, St. Jude Children's Research Hospital, 262 Danny Thomas Place, Memphis, TN 38105, USA
[2]Center for Proteomics and Metabolomics, St. Jude Children's Research Hospital, 262 Danny Thomas Place, Memphis, TN 38105, USA
[3]Department of Cell and Molecular Biology, St. Jude Children's Research Hospital, 262 Danny Thomas Place, Memphis, TN 38105, USA
[4]Department of Structural Biology, St. Jude Children's Research Hospital, 262 Danny Thomas Place, Memphis, TN 38105, USA
[5]Lead contact
*Correspondence: fabio.demontis@stjude.org
https://doi.org/10.1016/j.crmeth.2024.100875

MOTIVATION Eukaryotic cells have evolved complex functions via their compartmentalization into organelles and subcellular microenvironments. Such specialization of the cellular space enabled optimal function but also resulted in compartment-specific challenges to proteostasis. However, due to the paucity of tools, how subcellular proteostasis is regulated in physiological and pathological conditions remains largely uncharted. In this study, we generated *Drosophila* strains that ubiquitously express misfolding-prone Fluc^{DM} protein variants that have been engineered to localize to the nucleus and mitochondria, along with an untargeted variant that localizes primarily to the cytoplasm. By validating these tools in several contexts, we demonstrate that compartment-targeted Fluc^{DM} variants can be used to either perturb or to monitor subcellular proteostasis, depending on the experimental design.

SUMMARY

Loss of proteostasis is a hallmark of aging that underlies many age-related diseases. Different cell compartments experience distinctive challenges in maintaining protein quality control, but how aging regulates subcellular proteostasis remains underexplored. Here, by targeting the misfolding-prone Fluc^{DM} luciferase to the cytoplasm, mitochondria, and nucleus, we established transgenic sensors to examine subcellular proteostasis in *Drosophila*. Analysis of detergent-insoluble and -soluble levels of compartment-targeted Fluc^{DM} variants indicates that thermal stress, cold shock, and pro-longevity inter-organ signaling differentially affect subcellular proteostasis during aging. Moreover, aggregation-prone proteins that cause different neurodegenerative diseases induce a diverse range of outcomes on Fluc^{DM} insolubility, suggesting that subcellular proteostasis is impaired in a disease-specific manner. Further analyses with Fluc^{DM} and mass spectrometry indicate that pathogenic tau^{V337M} produces an unexpectedly complex regulation of solubility for different Fluc^{DM} variants and protein subsets. Altogether, compartment-targeted Fluc^{DM} sensors pinpoint a diverse modulation of subcellular proteostasis by aging regulators.

INTRODUCTION

Age-related diseases arise from interconnected, degenerative events that occur at multiple levels in organs, tissues, cells, and subcellular compartments.[1–5] Although the decline of proteostasis is a defining feature of many age-related diseases,[6–8] little is known about how protein quality control is regulated in different cellular organelles and compartments during aging.[1–3] Because each cellular compartment/organelle is characterized by its folding environment and proteolytic capacities, disease processes and environmental stressors that challenge protein quality control may impact each organelle differently.[1,2]

The previous development of tools in *C. elegans* and cell culture has provided remarkable insight into this subject. For example, redox reporters targeted to the endoplasmic reticulum (ER) and the cytoplasm indicate that the redox state of these cell compartments is profoundly remodeled during aging in *C. elegans*. Specifically, the ER is oxidizing in young animals but shifts toward reducing conditions during aging, whereas the cytosol becomes more oxidizing.[9] Another study used a general (i.e., cytoplasmic)

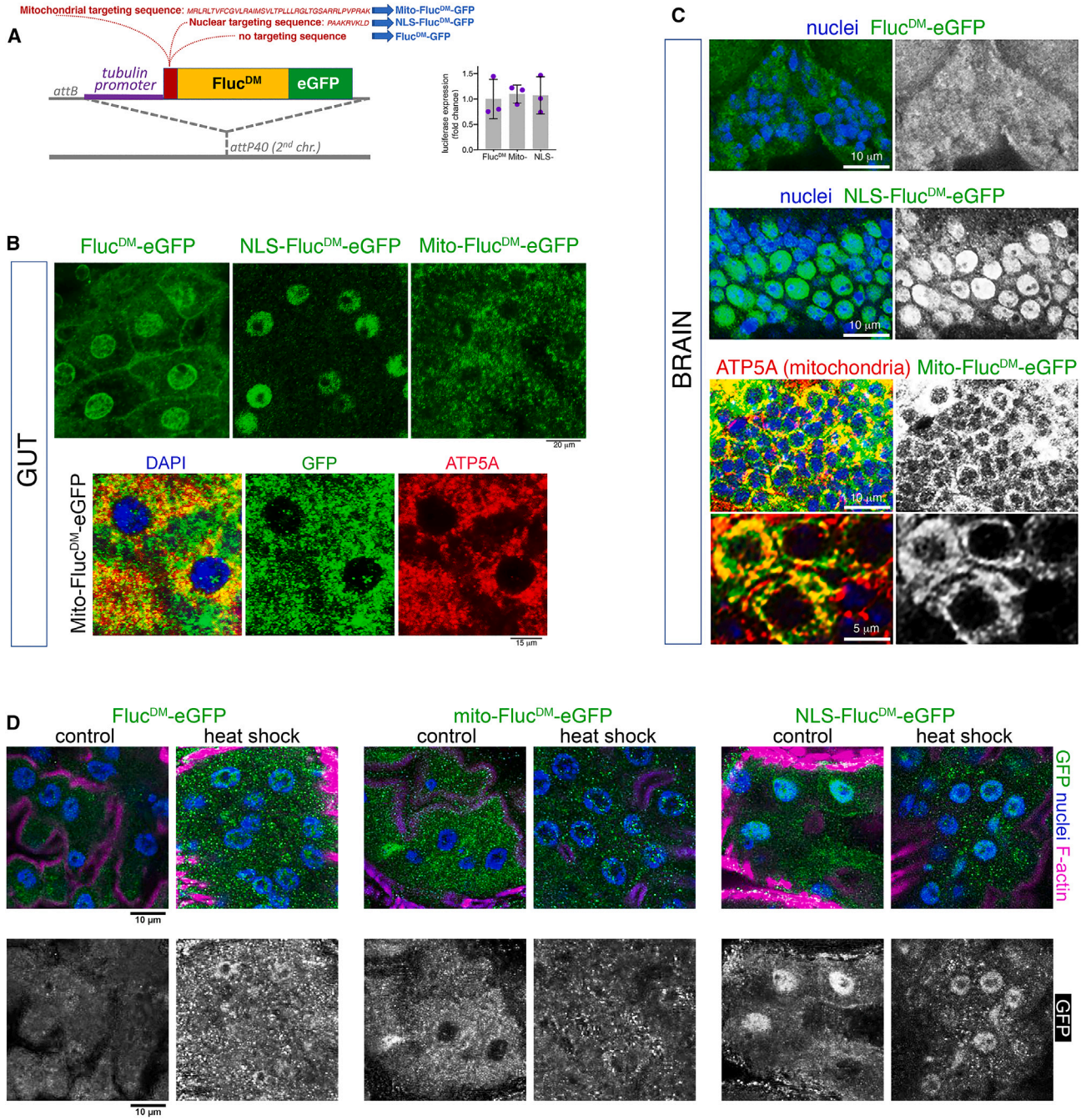

Figure 1. Generation of compartment-targeted, misfolding-prone Fluc^{DM} variants to perturb and sense subcellular proteostasis in *Drosophila*

(A) Generation of transgenic organelle-targeted sensors of protein quality control based on a misfolding-prone mutant firefly luciferase (Fluc^{DM}) fused to EGFP. The mitochondrial targeting sequence from the human mitochondrial COX VIII protein was utilized to generate the mito-Fluc^{DM} variant, whereas a standard nuclear targeting sequence was used to generate the NLS-Fluc^{DM}. General (untargeted) sensors and reporters for mitochondria and the nucleus were site integrated and are expressed ubiquitously (downstream of a tubulin promoter) and at similar levels, as indicated by qRT-PCR with 3 batches of flies and the mean ± SD (no significant changes, one-way ANOVA).

(B) Immunostaining and confocal microscopy of enterocytes indicate that Fluc^{DM} variants exhibit the expected specificity in subcellular localization. General (untargeted) Fluc^{DM} is detected in the cytoplasm (but also in the nucleus and plasma membrane), mito-Fluc^{DM} is detected in ATP5A-stained mitochondria, and NLS-Fluc^{DM} is found in the nucleus. Scale bars represent 20 and 15 µm, as indicated.

(C) Immunostaining and confocal microscopy of brain cells from the antennal lobe indicates a similar localization. The untargeted Fluc^{DM} is detected in the cytoplasm, mito-Fluc^{DM} is detected in ATP5A-positive mitochondria, and NLS-Fluc^{DM} is found in the nucleus. Scale bars represent 10 and 5 µm.

(legend continued on next page)

sensor of proteostasis based on a structurally destabilized firefly luciferase mutant ($Fluc^{DM}$) and found that aging leads to an increase in sensor insolubility in *C. elegans*.[10] Organelle-targeted sensors can also be used to identify organelle-specific components of proteostasis. For example, by using model substrates targeted to the nucleus and the cytoplasm, studies in yeast have unveiled that proteostasis in these compartments is regulated by distinct sets of proteins and that the ubiquilin Dsk2 is required to clear nuclearly misfolded proteins.[11] Moreover, compartment-specific sensors of proteostasis may also be used to monitor inter-organelle crosstalk, which is a component of age-related processes.[1,2,12–14] In addition to working as sensors, previous studies have found that misfolding-prone proteins[15,16] and organelle-targeted reporters such as mito-GFP[17] can impact the specific compartment where they are targeted and induce adaptive and maladaptive stress responses.[18–21] On this basis, depending on the experimental design, organelle-targeted reporter proteins may be utilized both as sensors of proteostasis or as probes to perturb proteostasis in a specific subcellular compartment.

Here, we expanded the toolkit to study subcellular proteostasis by generating transgenic *Drosophila* strains that express misfolding-prone firefly luciferase $Fluc^{DM}$ variants that localize to the mitochondria, the nucleus, and the cytoplasm. $Fluc^{DM}$ was chosen as the starting point for generating sensors of subcellular proteostasis because of the previous studies demonstrating its utility in other model organisms[10,22] and because it is an exogenous protein that may be less likely to perturb cellular functions compared to the transgenic expression of an endogenous misfolding-prone protein. By comparing the impact of experimental versus control interventions in the presence of each $Fluc^{DM}$, we find that $Fluc^{DM}$ variants can be utilized as sensors of proteostasis. By monitoring the levels of detergent-soluble and -insoluble $Fluc^{DM}$, we find that subcellular proteostasis is differentially regulated by environmental stress, endocrine signaling, and aggregation-prone proteins (such as microtubule-associated protein tau [MAPT]) during aging in *Drosophila*. Moreover, we find that these tools can be utilized to perturb proteostasis in a compartment-specific manner when a $Fluc^{DM}$ variant is compared to an isogenic control with no $Fluc^{DM}$ expression. Altogether, these studies indicate that organelle-targeted misfolding-prone proteins may find several experimental applications and that such tools may provide insight into how subcellular proteostasis is differentially cross-regulated in distinct compartments by age-related diseases and anti-aging interventions.

RESULTS

Establishment of transgenic, compartment-targeted, misfolding-prone $Fluc^{DM}$ proteins to sense and perturb subcellular proteostasis in *Drosophila*

$Fluc^{DM}$ is a misfolding-prone firefly luciferase protein variant that has been used as a reporter of cytoplasmic proteostasis in cell culture and in *C. elegans*[10] and, more recently, *in vivo* in mice.[22] Detergent-soluble $Fluc^{DM}$ is functional, whereas sequestration of $Fluc^{DM}$ into detergent-insoluble fractions (which typically correspond to protein aggregates) indicates the occurrence of misfolding and the consequent loss of solubility. In addition to increased misfolding, retention of $Fluc^{DM}$ into detergent-insoluble fractions can also indicate deficits in the degradation of misfolded proteins. In line with this model, aging increases $Fluc^{DM}$ insolubility in *C. elegans*,[10] confirming that cytoplasmic proteostasis declines with aging.[6,7,10,23]

Based on the previously characterized misfolding-prone luciferase,[10] we generated compartment-targeted $Fluc^{DM}$ variants tagged with enhanced green fluorescent protein (EGFP) for *in vivo* use in *Drosophila* (Figure 1A). To generate a $Fluc^{DM}$ variant targeted to mitochondria (mito-$Fluc^{DM}$-EGFP), the mitochondrial import sequence from the human mitochondrial COX VIII protein (cytochrome c oxidase subunit 8, a component of the respiratory chain located in the inner mitochondrial membrane)[24,25] was fused to the N terminus of $Fluc^{DM}$-EGFP. A standard nuclear targeting sequence (PAAKRVKLD)[26] was fused to the $Fluc^{DM}$ N terminus to generate a $Fluc^{DM}$-EGFP variant with a nuclear localization signal (NLS-$Fluc^{DM}$-EGFP). Lastly, transgenic flies were also generated for untargeted $Fluc^{DM}$-EGFP (Figure 1A), which has been found previously to display diffuse cytoplasmic localization in *C. elegans* and cell culture.[10]

To ensure expression in the physiological range, all $Fluc^{DM}$ variants were engineered to be expressed downstream of a ubiquitous tubulin promoter and to be site integrated at the same position into the genome via the phiC31 integrase system,[27] leading to similar expression levels, as assessed by qRT-PCR (Figure 1A).

Next, immunostaining and confocal microscopy were utilized to determine the subcellular localization of $Fluc^{DM}$ protein variants. Considering that the tubulin promoter drives the expression of $Fluc^{DM}$ transgenes ubiquitously, $Fluc^{DM}$ intracellular localization was monitored in enterocytes, which are a convenient system for these analyses given their large cell size, and in brain cells because of the importance of proteostasis for neurodegeneration.[7] Confocal microscopy indicates that $Fluc^{DM}$ variants exhibit distinct subcellular localization (Figures 1B and 1C): general (untargeted) $Fluc^{DM}$ is detected in the cytoplasm, nucleus, and plasma membrane of enterocytes (Figure 1B) but only in the cytoplasm of brain cells (Figure 1C); NLS-$Fluc^{DM}$ is detected in the nucleus of both enterocytes and brain cells (Figures 1B and 1C); and mito-$Fluc^{DM}$ is detected in mitochondria, defined by co-staining for the mitochondrial marker ATP5a (ATP synthase F1 subunit alpha) (Figures 1B and 1C). However, not all mito-$Fluc^{DM}$ is detected in mitochondria, presumably because mito-$Fluc^{DM}$ is synthesized in the cytosol, and its import into mitochondria is suboptimal. Altogether, we established transgenic *Drosophila* strains that express general (i.e., cytosolic) and compartment-targeted $Fluc^{DM}$ variants.

It has been found previously that heat shock results in the accumulation of cytoplasmic aggregates of $Fluc^{DM}$ in cell culture.[10] On this basis, we tested whether the intracellular localization of

(D) Immunostaining of enterocytes from heat-shocked and control flies identifies $Fluc^{DM}$-GFP aggregates that accumulate in the cytoplasm in response to thermal stress compared to non-heat-shocked controls. Similar heat-induced cytoplasmic aggregates are also found in heat-shocked NLS-$Fluc^{DM}$-EGFP and mito-$Fluc^{DM}$-EGFP cells. In the case of mito-$Fluc^{DM}$-EGFP, these aggregates are recognizable because they produce larger puncta than the staining that corresponds to mito-$Fluc^{DM}$-EGFP-positive mitochondria (B). Scale bar, 10 μm.

compartment-targeted Fluc^{DM} variants is remodeled by thermal stress. To this purpose, we examined the subcellular localization of the EGFP-tagged Fluc^{DM} variants by immunostaining the enterocytes of heat-shocked flies and controls with anti-GFP antibodies. In agreement with previous findings in cell culture,[10] the diffuse localization of the general Fluc^{DM}-EGFP sensor shifted to a spotty pattern upon heat shock, indicative of the sequestration of a fraction of the Fluc^{DM}-EGFP into cytoplasmic aggregates (Figure 1D). Similar cytoplasmic aggregates were also found in the heat-shocked NLS-Fluc^{DM}-EGFP and mito-Fluc^{DM}-EGFP cells (Figure 1D). In the case of mito-Fluc^{DM}-EGFP, these aggregates were recognized because they were bigger than the speckles that correspond to mitochondria with mito-Fluc^{DM}-EGFP (Figure 1D), which largely co-localizes with the mitochondrial marker ATP5a (Figures 1B and 1C). Altogether, these findings indicate that thermal stress induces the sequestration of a fraction of the Fluc^{DM} variants into cytoplasmic aggregates (Figure 1D).

Organism-wide perturbation of subcellular proteostasis with compartment-targeted Fluc^{DM} variants extends lifespan and delays neuromuscular aging

Protein misfolding restricted to a specific cell compartment has been found previously to induce adaptive and maladaptive responses locally and even systemically.[16,18–21] For example, the expression of a metastable sarcomeric protein in *C. elegans* skeletal muscle induces a local and systemic stress response characterized by transcriptional induction of the chaperone *Hsp90*.[15] Moreover, it was recently appreciated that expression of mito-GFP, a GFP with a mitochondrial import sequence that is utilized to identify mitochondria by microscopy, leads to perturbation of mitochondrial proteostasis and induction of the mitochondrial unfolded protein response.[17] On this basis, with an appropriate experimental design, Fluc^{DM} variants may be utilized to perturb proteostasis in a subcellular compartment and determine the corresponding stress responses induced by such compartment-restricted disruption of proteostasis compared to controls with no Fluc^{DM}.

To determine the overarching results of perturbing proteostasis in distinct subcellular compartments at the organism level, we examined whether Fluc^{DM} variants regulate lifespan and neuromuscular function during aging compared to isogenic controls with no Fluc^{DM} expression. Survival analyses indicate that Fluc^{DM} variants extend lifespan, although this occurs differently for each compartment-targeted Fluc^{DM}: at 18°C and 25°C, the lifespan extension is more pronounced for the untargeted (i.e., cytoplasmic) Fluc^{DM} and for mito-Fluc^{DM} compared to NLS-Fluc^{DM} (Figures 2A and 2B). However, all Fluc^{DM} variants similarly extend lifespan at 29°C (Figure 2C), a temperature that corresponds to mild chronic thermal stress for *Drosophila*. Interestingly, 2 copies of the mito-Fluc^{DM} and NLS-Fluc^{DM} transgenes were not more effective in extending lifespan than single copies, suggesting that an optimal adaptive response is already reached with 1 copy and that additional copies of the transgene may not further induce the response or even be detrimental (Figures 2A–2C).

We next examined negative geotaxis; i.e., the startle-induced escape response from gravity.[28–30] This is an innate behavior that depends on the function of the brain and skeletal muscle and that senesces with aging in *Drosophila*.[28–30] These studies indicate that the percentage of flies able to climb progressively decreases with aging in control flies but less so in isogenic flies that express untargeted Fluc^{DM}, mito-Fluc^{DM}, and NLS-Fluc^{DM} at 18°C, 25°C, and 29°C (Figures 2D–2F). Altogether, these findings indicate that organism-wide expression of a misfolding-prone protein targeted to distinct cell compartments induces, to varying degrees, a hormetic response that extends lifespan and preserves neuromuscular function during aging in *Drosophila*.

It has been shown previously that metastable proteins can trigger an adaptive response that partially preserves or even restores protein quality control.[18–21] On this basis, we next tested whether Fluc^{DM} variants regulate proteostasis in a Huntington's disease model based on the expression of GFP-tagged pathogenic huntingtin in the retina and in which Htt-polyQ72-GFP aggregates progressively form with aging.[31–34] Compared with control mCherry and with no transgene expression, all Fluc^{DM} variants significantly reduced Htt-polyQ72-GFP aggregates (Figure 2G), suggesting that the stress response induced by Fluc^{DM} improves proteostasis compared to control flies with no Fluc^{DM} expression.

In summary, these studies indicate that compartment-targeted Fluc^{DM} variants can be utilized to perturb subcellular proteostasis and to identify the consequent hormetic stress responses that are induced compared to isogenic controls with no Fluc^{DM} expression.

Transcriptional stress responses induced by organelle-targeted perturbation of proteostasis with Fluc^{DM} variants

Having established that Fluc^{DM} variants induce a non-canonical stress response at the organismal and cellular levels (Figure 2), we next sought to define the underlying transcriptional responses. To this purpose, RNA sequencing (RNA-seq) was done from Fluc^{DM} variants and isogenic control flies reared at 18°C, 25°C, and 29°C (Table S1).

Heatmaps of the genes with the highest *Z* scores indicate that Fluc^{DM} flies display substantial gene expression changes compared to isogenic controls with no Fluc^{DM} (Figure 3A). Analysis of the Gene Ontology (GO) terms that are modulated by Fluc^{DM} include several categories involved in proteostasis and aging, such as proteases, lipid metabolism, and innate immunity (Figure 3B). Examples of differentially regulated genes include the mitochondrial heat shock protein 22 (Hsp22),[35] which is among the most highly induced genes in all Fluc^{DM} strains compared to isogenic controls: while *Hsp22* expression normally rises with heat from 18°C to 29°C (Figure 3C), Fluc^{DM} further significantly increases its levels both at 25°C and 29°C. Because previous studies have found a key role for Hsp22 in lifespan regulation,[35] these findings suggest that Hsp22 is part of the Fluc^{DM}-induced stress response that extends lifespan and improves neuromuscular function (Figure 2). Consistent with this model, NLS-Fluc^{DM}, which improved climbing and lifespan less than Fluc^{DM} and mito-Fluc^{DM} (Figure 2), induced *Hsp22* expression less than the other Fluc^{DM} variants (Figure 3C). Additional Fluc^{DM}-regulated genes include the APP (amyloid precursor protein)-cleaving beta-secretase *Bace* (which is downregulated by Fluc^{DM}) and the ubiquitin ligase *CG32581/sordd2* (suppression of retinal degeneration disease 1 upon overexpression 2), which

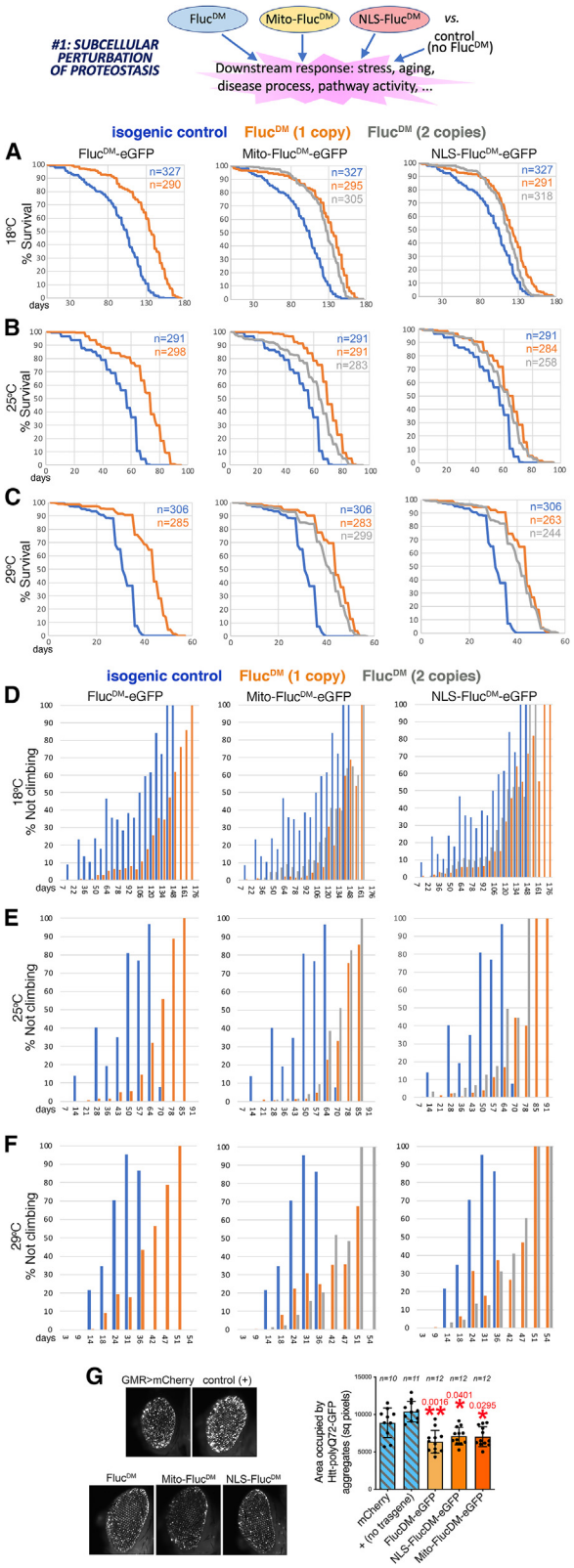

Figure 2. Use of compartment-targeted Fluc^{DM} variants to perturb subcellular proteostasis

Fluc^{DM} are misfolding-prone proteins and, therefore, they may challenge proteostasis in the subcellular compartment to which they are targeted. On this basis, Fluc^{DM} variants can be used as tools to induce a moderate perturbation of subcellular proteostasis when compared to an isogenic control with no Fluc^{DM} expression.

(A–C) The untargeted (cytoplasmic) Fluc^{DM}, the mitochondrially targeted mito-Fluc^{DM}, and the nucleus-targeted NLS-Fluc^{DM} extend lifespan ($p < 0.001$, log -rank test, with n indicated) when compared to isogenic controls with no Fluc^{DM}. Distinct Fluc^{DM} variants have effects of different magnitudes; the untargeted Fluc^{DM} is more effective in extending lifespan at 18°C (A) and at 25°C (B) compared to NLS-Fluc^{DM}, whereas similar lifespan extension is seen at 29°C (C) for all Fluc^{DM} variants. These findings suggest that moderate perturbation of subcellular proteostasis by Fluc^{DM} variants induces a stress response that extends lifespan. A single (orange) or 2 copies (gray) of the Fluc^{DM} transgenes similarly extend lifespan compared to the isogenic controls with no Fluc^{DM} (blue).

(D–F) Negative geotaxis assays indicate that expression of misfolding-prone Fluc^{DM} proteins targeted to distinct subcellular compartments reduces age-related neuromuscular dysfunction during aging compared to isogenic controls that do not express Fluc^{DM}. A similar protection is found at 18°C (D), 25°C (E), and 29°C (F). These findings suggest that moderate perturbation of subcellular proteostasis by compartment-targeted Fluc^{DM} variants induces an adaptive stress response that improves neuromuscular function; $p < 0.001$ (log -rank test) with n indicated (A–C).

(G) Aggregates of GFP-tagged pathogenic huntingtin-polyQ can be seen in the retina of *GMR>Htt-polyQ72-GFP* flies at 30 days of age, but the total area of such aggregates is higher in controls (mCherry and no transgene, +) compared to flies that express Fluc^{DM} variants. This suggests that moderate stress induced by Fluc^{DM} can induce a hormetic stress response that improves proteostasis. The n (biological replicates) and the mean ± SD are indicated, with $^{*}p < 0.05$ and $^{**}p < 0.01$ (one-way ANOVA).

is homologous to human RNF185 (ring finger protein 185) and is highly induced by all Fluc^{DM} variants (Figure 3C).

Further analysis of the transcriptional responses induced by mito-Fluc^{DM} and NLS-Fluc^{DM} compared to the untargeted Fluc^{DM} revealed several gene categories that are differentially regulated by distinct Fluc^{DM} proteins: lipid metabolism and antimicrobial peptides were commonly induced by mito-Fluc^{DM} and NLS-Fluc^{DM} compared to the untargeted Fluc^{DM}, whereas components of the ER and gustatory receptors were enriched categories among the genes regulated by mito-Fluc^{DM} and by NLS-Fluc^{DM}, respectively (Figure 3D). An example of gene that is differentially regulated by distinct Fluc^{DM} variants is the triacylglycerol lipase *CG11598*, which is homologous to human LIPN (lipase family member N) and related lipases: *CG11598* is more highly expressed in NLS-Fluc^{DM} versus mito-Fluc^{DM} and even more so compared to the untargeted Fluc^{DM} (Figure 3E). Altogether, transcriptional profiling identifies differentially expressed genes that are induced consistently or distinctly by Fluc^{DM} variants compared to isogenic controls with no Fluc^{DM} expression.

Compartment-targeted Fluc^{DM} sensors indicate that heat and cold shock distinctly impact subcellular proteostasis

In addition to perturbing proteostasis in subcellular compartments (Figures 2 and 3), Fluc^{DM} variants are primarily utilized as sensors of proteostasis, as found previously for a general (i.e., cytoplasmic) Fluc^{DM} in *C. elegans*[10] and for compartment-targeted Fluc^{DM} in mice.[22] To test whether this is also possible in

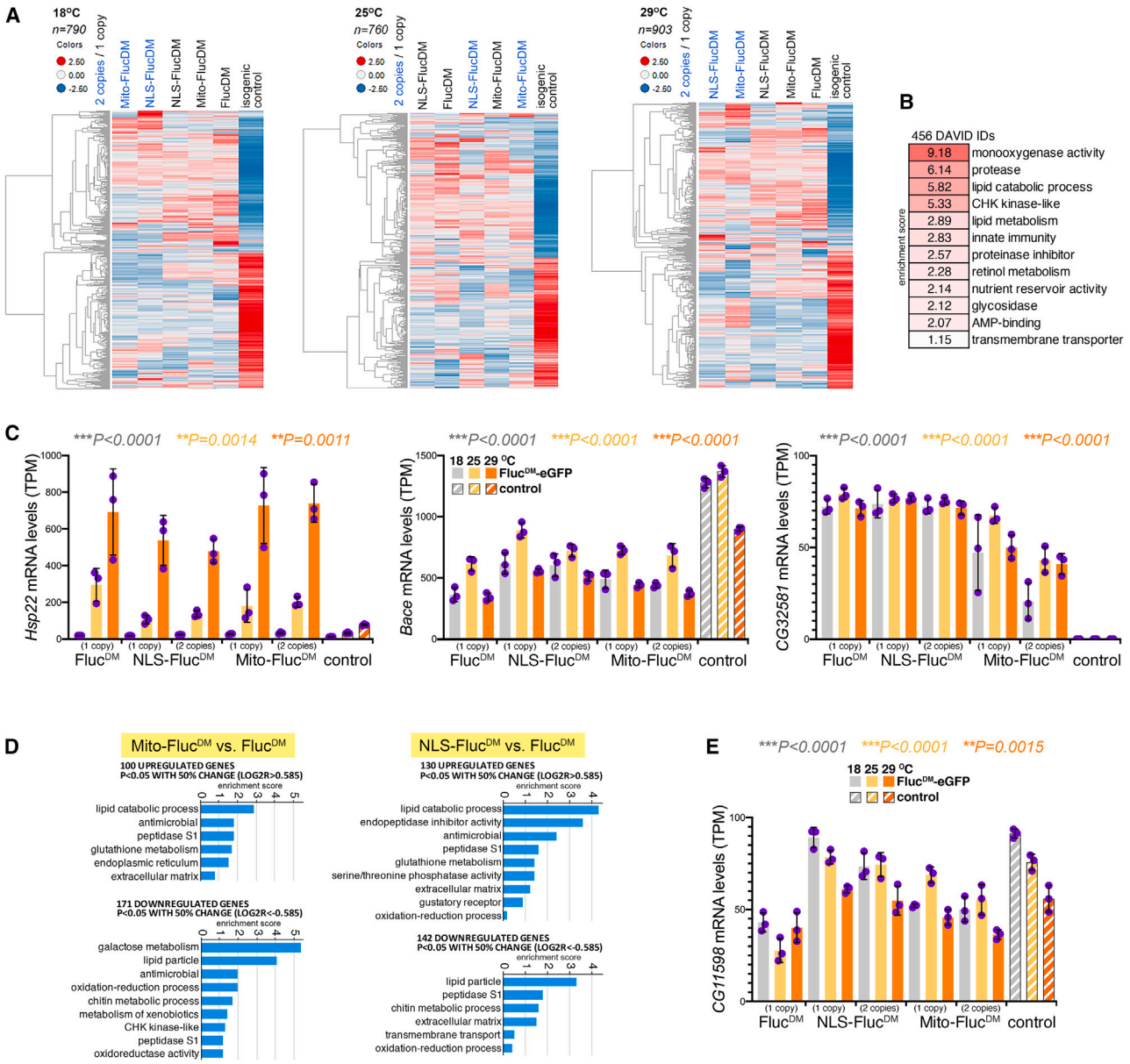

Figure 3. Compartment-targeted Fluc^{DM} variants induce a transcriptional stress response compared to isogenic controls with no Fluc^{DM}

(A) Heatmap of the genes that are most differentially regulated indicate that Fluc^{DM} variants induce transcriptional adaptive responses that differentiate them from isogenic controls with no Fluc^{DM} expression. The average *Z* scores are color coded; upregulated genes are shown in red and downregulated genes in blue.

(B) Several gene categories are commonly modulated by compartment-targeted Fluc^{DM} variants, including genes that encode for proteins with monooxygenase activity, proteases, and proteins involved in lipid catabolism.

(C) Differentially modulated genes such as *Hsp22*, *Bace*, and *CG32581/sordd2* may provide a mechanistic explanation for how stress responses induced by perturbation of subcellular proteostasis are protective during aging (Figure 2).

(D) Apart from transcriptional stress responses that are commonly induced by all Fluc^{DM} variants (B and C), there are also gene categories that are differentially regulated by mito-Fluc^{DM} and by NLS-Fluc^{DM} versus the untargeted Fluc^{DM}.

(E) An example of a gene that is differentially modulated by distinct Fluc^{DM} variants is the triacylglycerol lipase CG11598, which is not regulated by NLS-Fluc^{DM}, is downregulated by mito-Fluc^{DM}, and even more downregulated by the untargeted Fluc^{DM} compared to isogenic controls with no Fluc^{DM} expression.

In (C) and (E), $n = 3$ (biological replicates) with the mean ± SD indicated; for each genotype, the mRNA levels (transcripts per million [TPM]) at 18°C (gray), 25°C (yellow), and 29°C (orange) are shown. For the genes in (C) and (E), the color-coded *p* value summary (one-way ANOVA) is reported for the comparison of Fluc^{DM} variants to the control at each temperature. Additional statistical cross-comparisons of each Fluc^{DM} to the control at each temperature are reported in the source data file (Table S4).

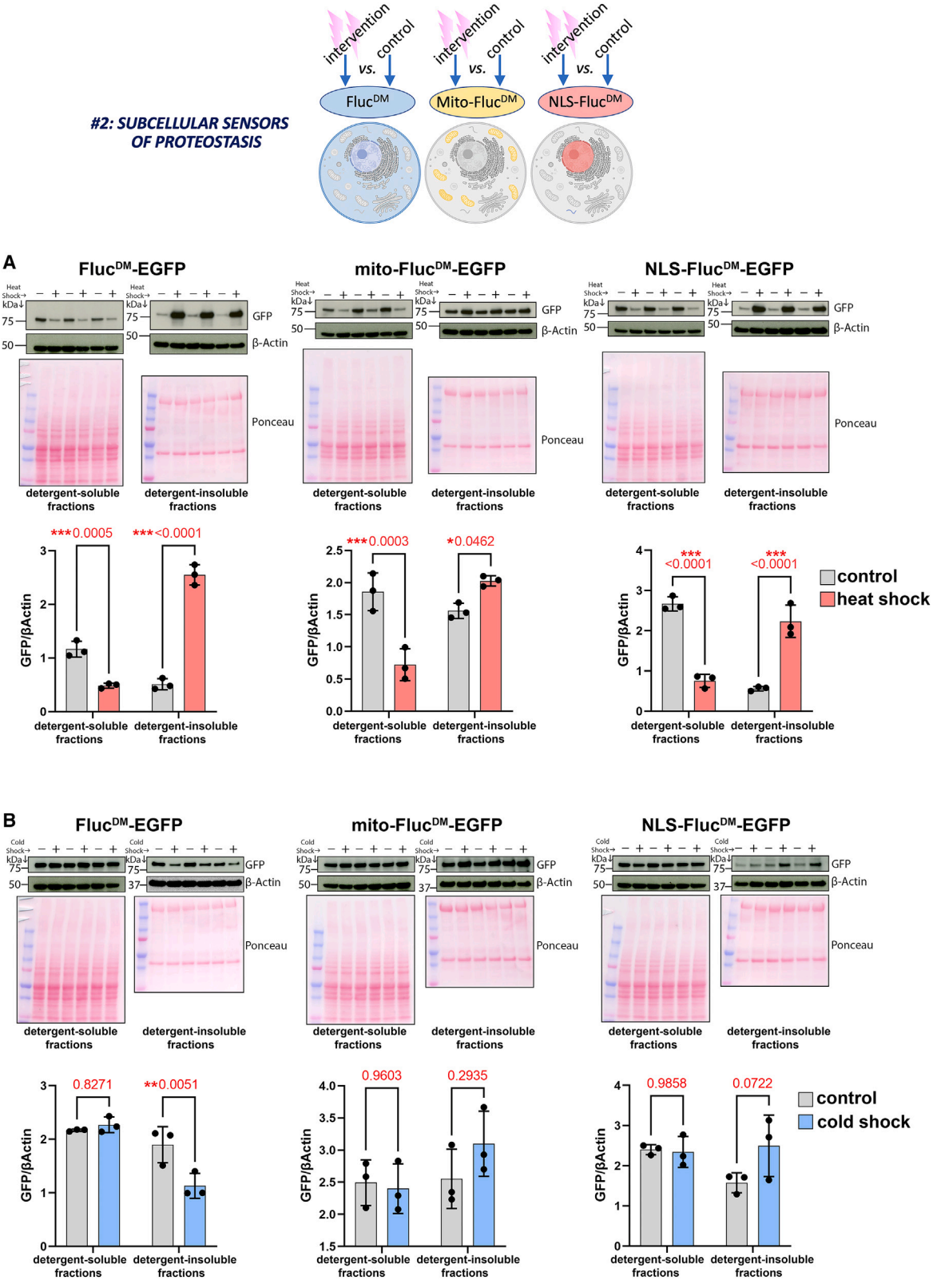

(legend on next page)

Drosophila, two environmental stressors (cold and heat shock) were utilized to determine how they impact subcellular proteostasis *in vivo*. While thermal stress (heat shock) is a well-known challenge to proteostasis because of heat-induced protein unfolding,[36–38] cold shock has been conversely found to improve proteostasis and delay aging.[39–43] However, the impact of cold and heat shock on subcellular proteostasis remains largely unexplored. To address this question, Fluc^{DM} strains were exposed to heat stress (36°C for 3 h) or cold shock (4°C for 2 h) and compared to isogenic controls kept at the standard temperature of 25°C. Subsequently, the solubility of the untargeted (i.e., cytoplasmic) Fluc^{DM}, the mitochondrial mito-Fluc^{DM}, and the nuclear NLS-Fluc^{DM} was analyzed via western blot of detergent-soluble and -insoluble fractions. As expected based on its capacity to cause protein unfolding,[36,37] thermal stress induced profound changes in Fluc^{DM} solubility that were, however, of different magnitudes in distinct subcellular compartments. In general, there was a decrease in the soluble levels of all Fluc^{DM} variants and a corresponding increase in their detergent-insoluble levels; these heat-induced changes in protein insolubility were the highest for the untargeted (i.e., cytoplasmic) Fluc^{DM}, intermediate for the nuclear NLS-Fluc^{DM}, and minimal for the mitochondrial mito-Fluc^{DM} (Figure 4A). Altogether, these findings suggest that certain cellular compartments (e.g., mitochondria) may be relatively resilient to heat-induced protein unfolding compared to the nucleus and the cytoplasm.

Cold shock impacts the cell differently than thermal stress.[39–43] Consistent with this scenario, western blots indicated that there were no changes in the soluble levels of any Fluc^{DM} variants, whereas the detergent-insoluble levels were conversely regulated depending on the compartment (Figure 4B): detergent-insoluble levels of the (cytoplasmic) Fluc^{DM} were reduced by cold shock but trended toward increasing for NLS-Fluc^{DM}, whereas minimal changes were found for mito-Fluc^{DM} (Figure 4B). Altogether, the folding status of compartment-targeted Fluc^{DM} variants indicates that proteostasis is affected differentially by heat and cold shock in distinct subcellular compartments.

The solubility of compartment-targeted Fluc^{DM} proteins is correspondingly regulated by cytoplasmic and mitochondrial chaperones

Proteostasis in distinct subcellular compartments critically relies on dedicated proteolytic systems and chaperones, such as the mitochondrial chaperone Hsp22 and the cytoplasmic chaperone Hsp70.[35,44–46] On this basis, we tested whether modulation of Hsp22 and Hsp70 impacts the folding status of Fluc^{DM} variants. Knockdown of Hsp70 resulted in an ~70% decline in Hsp70 mRNA levels (Figure S1A) and in a significant decline in the detergent-soluble levels of the untargeted (i.e., cytoplasmic) Fluc^{DM} (Figure S1B), whereas there were no changes in the detergent-soluble and -insoluble levels of mito-Fluc^{DM} and NLS-Fluc^{DM} (Figures S1C and S1D). Moderate (~3-fold) overexpression of the mitochondrial chaperone *Hsp22* (Figure S1A) did not significantly affect the detergent-soluble and -insoluble levels of Fluc^{DM} and NLS- Fluc^{DM} (Figures S2A and S2C) but significantly reduced the levels of detergent-insoluble mito-Fluc^{DM} (Figure S2B), consistent with the known role of Hsp22 in preserving mitochondrial proteostasis.[35] Altogether, these findings indicate that chaperones with specific subcellular localizations correspondingly impact the folding status of the Fluc^{DM} sensors that are targeted to the same subcellular compartment.

Previous studies in *C. elegans* have found that aging leads to an increase in Fluc^{DM} sensor insolubility.[10] On this basis, we examined whether the detergent-soluble and -insoluble levels of Fluc^{DM} variants are modulated by aging in extracts from whole flies, heads (enriched for tissues of the central nervous system), and thoraces (enriched for skeletal muscle). In whole flies, there was a significant increase in the detergent-insoluble levels of the untargeted (i.e., cytoplasmic) Fluc^{DM} sensor with aging, whereas mito-Fluc^{DM}, and NLS-Fluc^{DM} were not modulated (Figure S3). Analysis of extracts from heads and thoraces indicates that there are minimal or no changes in the insoluble levels of Fluc^{DM}, mito-Fluc^{DM}, and NLS-Fluc^{DM} during aging (Figure S3).

Similar results were also found by monitoring the folding status of the firefly luciferase Fluc^{DM}-GFP sensors with luciferase assays: the signal for Fluc^{DM} does not significantly change with aging (10, 30, and 60 days) in fly thoraces. Moreover, the luciferase signal (normalized by total protein content) was higher for the general Fluc^{DM} compared to NLS-Fluc^{DM} and mito-Fluc^{DM}, suggesting that there could be detection limits that can impair the use of luciferase assays for monitoring the folding status of Fluc^{DM} variants (Figure S4).

Altogether, these findings indicate that the folding status of Fluc^{DM} variants is relatively well preserved in the cytoplasm, nucleus, and mitochondria of aging cells in *Drosophila* in the absence of environmental shocks or genetic perturbations.

Figure 4. Use of compartment-targeted Fluc^{DM} as sensors of subcellular proteostasis

Fluc^{DM} are misfolding-prone proteins and, therefore, can be used to determine whether an experimental intervention modulates proteostasis compared to a control intervention. Specifically, Fluc^{DM} protein misfolding leads to its detergent insolubility, which indicates defects in protein quality control.

(A) Testing compartment-targeted Fluc^{DM} with thermal stress (red) versus controls (gray). Western blots of detergent-soluble and -insoluble fractions from whole flies with anti-GFP antibodies detect the EGFP-tagged Fluc^{DM} variants targeted to the mitochondria (mito-Fluc^{DM}) and the nucleus (NLS-Fluc^{DM}) and the untargeted Fluc^{DM} that localizes primarily to the cytoplasm. Ponceau staining and β-actin are shown as normalization controls, and the graphs refer to the GFP levels normalized by β-actin. Heat shock significantly decreases the detergent-soluble levels of all compartment-targeted Fluc^{DM}. This corresponds to an increase in the detergent-insoluble levels of the untargeted (i.e., cytoplasmic) Fluc^{DM}, NLS-Fluc^{DM}, and, to a lower extent, mito-Fluc^{DM}. Altogether, these findings indicate that thermal stress compromises proteostasis across the cell but more prominently in the cytoplasm and nucleus compared to the mitochondria. $n = 3$ (biological replicates) with the mean ± SD indicated; $^{*}p < 0.05$ and $^{***}p < 0.001$ (unpaired two-tailed t test).

(B) Testing compartment-targeted Fluc^{DM} with cold shock (blue) versus controls (gray). Shown are western blots of detergent-soluble and -insoluble fractions from whole flies with anti-GFP and anti-β-actin antibodies. Cold shock reduces the detergent-insoluble levels of the untargeted (i.e., cytoplasmic) Fluc^{DM}, whereas there are no changes in the detergent-soluble levels and in the detergent-insoluble levels of mito-Fluc^{DM} and NLS-Fluc^{DM}. Altogether, these findings indicate that cold shock improves cytoplasmic proteostasis but does not impact protein quality control in the nucleus and mitochondria. $n = 3$ (biological replicates) with the mean ± SD indicated; $^{**}p < 0.01$ (unpaired two-tailed t test).

Modulation of subcellular proteostasis by endocrine signaling during aging

Aging is characterized by changes in multiple organ systems that collectively decrease the ability of the organism to maintain homeostasis.[6,47–49] Previous studies have shown that inter-organ endocrine signaling regulates systemic aging and lifespan.[50–59] Skeletal muscle has emerged as an important tissue in the systemic regulation of aging because of its capacity to secrete a variety of signaling factors (myokines) that contribute to inter-organ signaling in response to exercise, stress, and nutrient sensing.[60–68] On this basis, we tested the function of the stress-induced amylase Amyrel, which regulates protein quality control in the central nervous system during aging via endocrine maltose/SLC45 signaling,[68,69] and the adipokinetic hormone (Akh), a glucagon-like hormone that antagonizes insulin signaling and delays aging.[70–72] In these studies, detergent-soluble and -insoluble fractions from whole flies were examined to determine the systemic outcome of muscle-expressed Akh. A ~4-fold overexpression of *Akh* in muscle (Figure S1A) did not impact the detergent-soluble and -insoluble levels of Fluc^{DM} and mito-Fluc^{DM} (Figures 5A and 5B), apart from a significant reduction in the soluble levels of Fluc^{DM} in old age (Figure 5A). However, overexpression of *Akh* in muscle significantly reduced the detergent-insoluble levels of NLS-Fluc^{DM} across all ages (Figure 5C), indicating that muscle-derived Akh improves nuclear proteostasis. Altogether, these findings indicate that signaling by the glucagon-like hormone Akh has a compartment-specific effect on subcellular proteostasis during aging.

We next tested whether another endocrine regulator of aging, Amyrel/maltose signaling,[69] similarly impacts subcellular proteostasis. In these studies, detergent-soluble and -insoluble fractions from heads and thoraces were examined to determine the outcome of muscle-expressed Amyrel on the central nervous system (head extracts) or skeletal muscle (thoraces). Western blots of detergent-soluble and -insoluble fractions indicate that muscle-specific induction of Amyrel reduces the insoluble levels of the untargeted (i.e., cytoplasmic) Fluc^{DM} in heads (Figure 5D), whereas mito-Fluc^{DM} and NLS-Fluc^{DM} are not affected (Figures 5E and 5F). These findings, therefore, indicate that Amyrel promotes proteostasis in the cytoplasm but not in the mitochondria and nuclei, which is consistent with the previous finding that Amyrel induces the expression of the cytoplasmic chaperone *Hsp23*.[69] Apart from the preservation of cytoplasmic proteostasis in head extracts (i.e., central nervous system), there was no effect of muscle-induced Amyrel on muscle proteostasis, as assessed from the analysis of detergent-soluble and insoluble levels of Fluc^{DM}, mito-Fluc^{DM}, and NLS-Fluc^{DM} in thoracic fractions (Figure S5). This is consistent with previous findings that have shown that overexpression of the maltose-producing enzyme Amyrel in skeletal muscle regulates protein quality control in the brain and retina but not in skeletal muscle during aging,[69] presumably because of the high expression of SLC45 maltose transporters in the brain versus the skeletal muscle.[69] Altogether, these findings indicate that anti-aging endocrine interventions may act by selectively improving proteostasis in specific subcellular compartments.

Divergent modulation of subcellular proteostasis by distinct aggregation-prone proteins

Aggregation-prone proteins are the culprits of several age-related diseases.[23,73–77] Although they are primarily localized in a specific cell compartment, aggregation-prone proteins perturb the function of many organelles.[1–3,14,78,79] However, it remains largely unknown whether such changes in cell function arise from corresponding changes in the protein quality control of subcellular compartments. To address this question, we monitored how the solubility of Fluc^{DM}, mito-Fluc^{DM}, and NLS-Fluc^{DM} is modulated by aggregation-prone proteins in skeletal muscle, an abundant tissue in which proteostasis is compromised with aging.[8,32,33,63] In particular, we utilized flies that express a protein with 49(GGGGCC) repeats that model those found in human C9orf72 and that are associated with the etiology of amyotrophic lateral sclerosis and frontotemporal dementia.[80] Such a protein with 49(GGGGCC) repeats forms toxic cytoplasmic and nuclear protein aggregates[81] compared to a control non-toxic protein with 8(GGGGCC) repeats[80] and to mCherry. Western blots of detergent-soluble and -insoluble fractions indicate that 49(GGGGCC) increases the insoluble levels of all Fluc^{DM} reporters (Fluc^{DM}, mito-Fluc^{DM}, and NLS-Fluc^{DM}) compared to the non-toxic controls, 8(GGGGCC)-containing proteins, and/or mCherry (Figures 6A–6C). Altogether, these findings indicate that a toxic protein with 49(GGGGCC) repeats compromises proteostasis widely across the cell in the cytoplasm, mitochondria, and the nucleus (Figures 6A–6C).

In a second set of studies, we expressed a C-terminal fragment of the human Machado-Joseph disease/spinocerebellar ataxia type 3 protein with a 78-repeat polyglutamine tract expansion (hATXN3.tr-Q78),[82] which forms toxic aggregates that are primarily located in the nucleus.[83–85] As a control, hATXN3.tr-Q78 was compared to a non-toxic hATXN3 with only 27 repeats (hATXN3.tr-Q27)[82] and to mCherry. These analyses indicate that hATXN3.tr-Q78 has no substantial effect on the solubility of the untargeted (i.e., cytoplasmic) Fluc^{DM} reporter (Figure 6D). There was minimal impact of hATXN3.tr-Q78 on the solubility of mito-Fluc^{DM} and NLS-Fluc^{DM}, and these effects were inconsistent when comparing hATXN3.tr-Q78 to distinct controls, hATXN3.tr-Q27 and mCherry (Figures 6E and 6F). Altogether, pathogenic ataxin-3 seems to minimally impact the folding status of Fluc^{DM} sensors located in distinct cell compartments, suggesting that pathogenic ataxin-3 may have a relatively limited impact on subcellular proteostasis.

In summary, the findings indicate that distinct pathogenic proteins have strikingly different impacts on subcellular protein quality control: while a toxic protein with 49(GGGGCC) repeats widely disrupts proteostasis in the cytoplasm, nucleus, and mitochondria, pathogenic ataxin-3 has minimal influence on the folding status of Fluc^{DM} proteins targeted to these compartments.

Compartment-specific effects of pathogenic tau on subcellar proteostasis during aging in *Drosophila*

Aggregation of MAPT deranges proteostasis, and it is a cause of Alzheimer's disease and related dementias.[86–88] While tau is a cytoplasmic protein, many other cell compartments, such as the nucleus and mitochondria, are perturbed by pathogenic

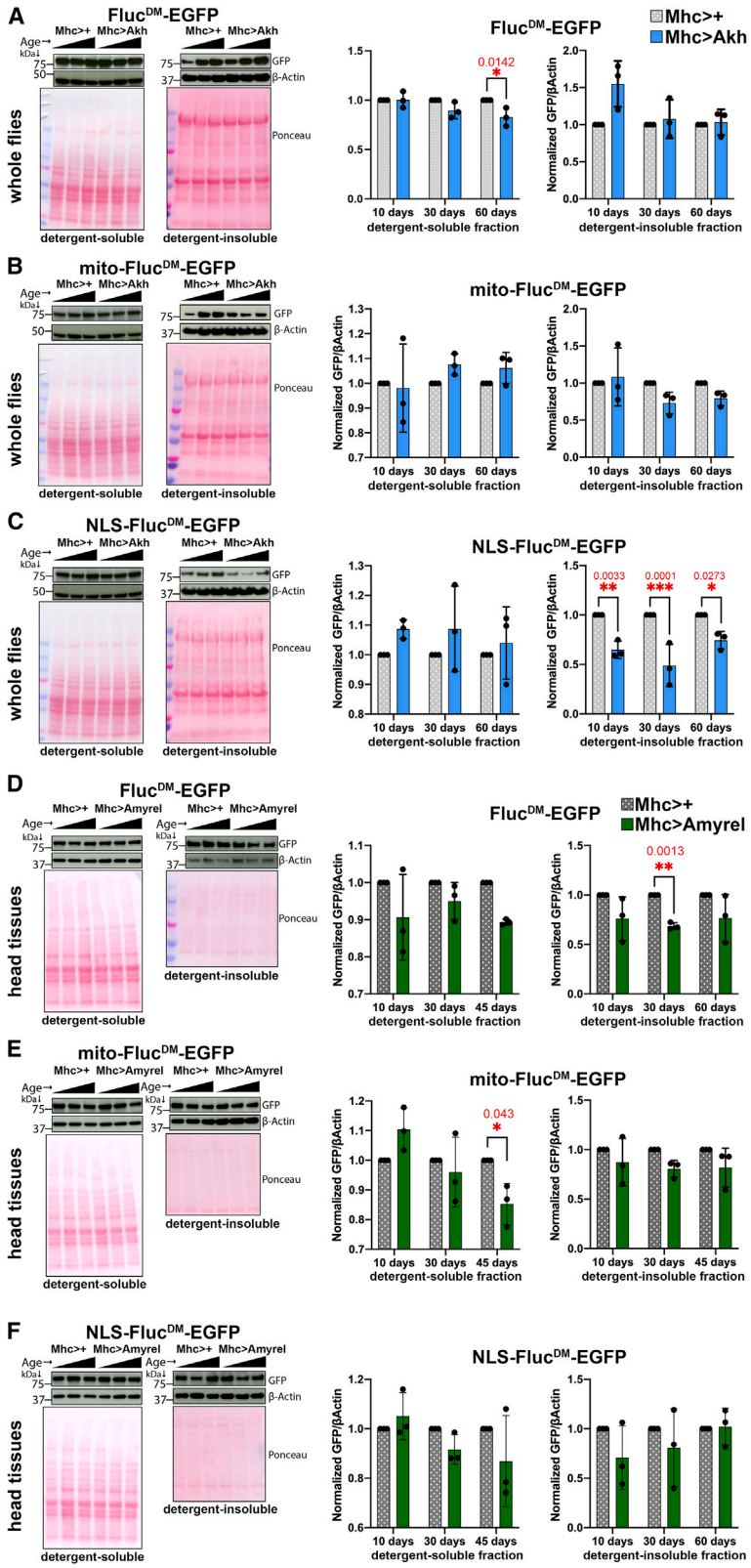

Figure 5. Organelle-targeted sensors of proteostasis indicate that distinct endocrine signaling factors differentially impact subcellular proteostasis

(A–C) Western blot analyses of detergent-soluble and insoluble fractions from control whole flies (*Mhc*>+, gray) and isogenic flies with muscle-specific overexpression of Akh (*Mhc>Akh*, blue), the *Drosophila* functional homolog of glucagon and related peptides. Western blotting with anti-GFP antibodies indicates the levels of Fluc^{DM}-EGFP sensors, whereas Ponceau staining and β-actin are used as normalization controls. Akh differentially impacts the detergent-insoluble levels of Fluc^{DM}-EGFP variants targeted to distinct cell compartments during aging. Akh reduces the detergent-insoluble levels of nuclearly localized NLS-Fluc^{DM} at all ages (C), whereas it does not substantially impact the detergent-insoluble levels of cytoplasmic Fluc^{DM} (A) and mitochondrial mito-Fluc^{DM} (B). The ages analyzed for each genotype are 10, 30, and 60 days. $n = 3$ (biological replicates) with the mean ± SD indicated; $^{*}p < 0.05$, $^{**}p < 0.01$, $^{***}p < 0.001$ (unpaired two-tailed t test).

(D–F) Western blot analysis of detergent-soluble and insoluble fractions from head extracts (enriched for the CNS) from control flies (*Mhc*>+, gray) and isogenic flies with muscle-specific overexpression of Amyrel (*Mhc>Amyrel*, green), which preserves proteostasis via maltose/SLC45 signaling. Amyrel reduces the detergent-insoluble levels of the untargeted (i.e., cytoplasmic) Fluc^{DM} (D) but not of mito-Fluc^{DM} (E) or NLS-Fluc^{DM} (F). Altogether, these findings indicate that muscle-derived Amyrel improves cytoplasmic proteostasis in the CNS. The ages analyzed for each genotype are 10, 30, and 45 days. $n = 3$ (biological replicates) with the mean ± SD indicated; $^{*}p < 0.05$, $^{**}p < 0.01$ (unpaired two-tailed t test).

CellPress
OPEN ACCESS

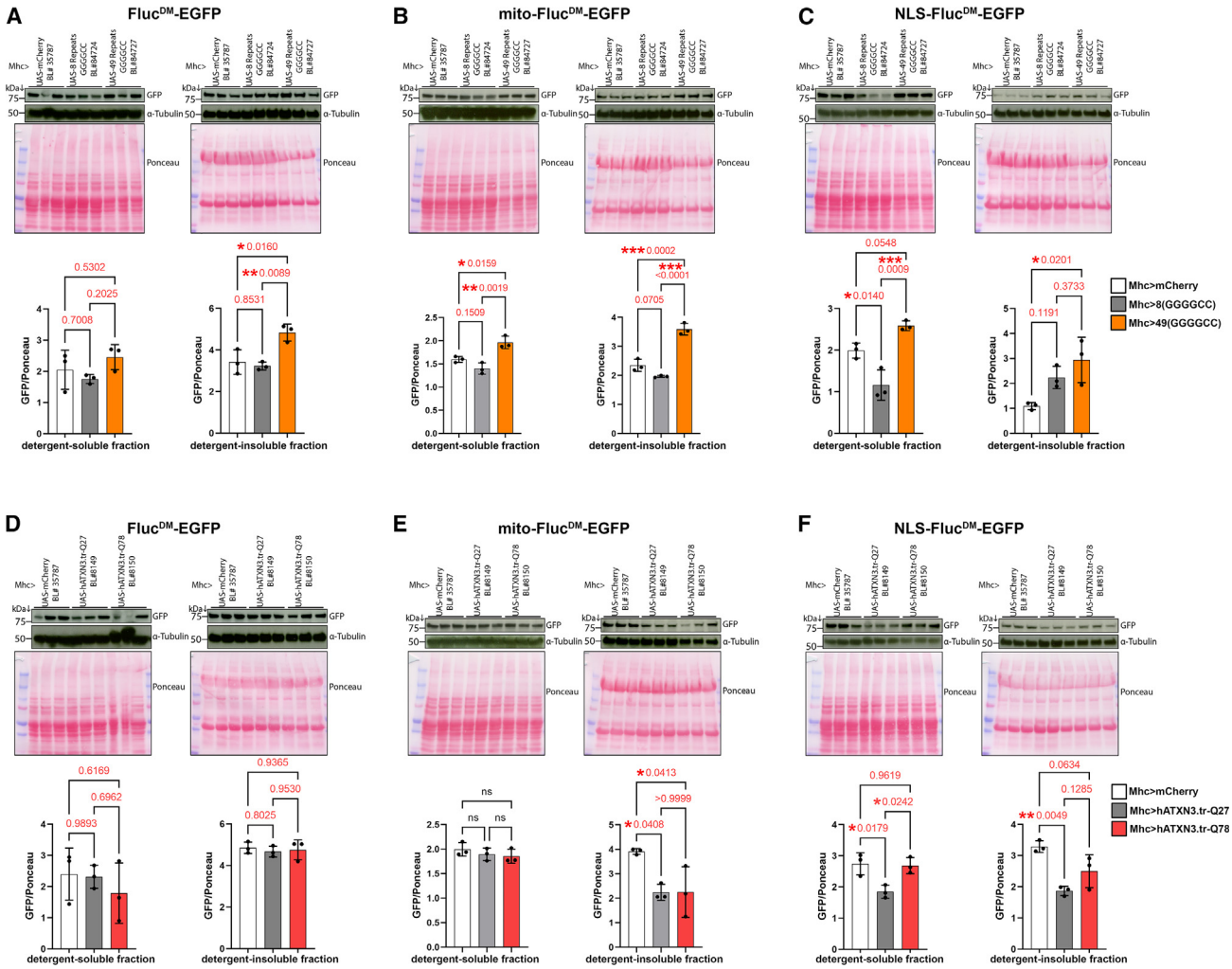

Figure 6. Distinct aggregation-prone proteins differentially impact subcellular proteostasis

(A–C) Analyses of detergent-soluble and insoluble fractions from skeletal muscle from 10-day-old flies that express a toxic, aggregation-prone protein with 49(GGGGCC) repeats (orange) compared to non-toxic controls, 8(GGGGCC)-containing proteins (gray), and/or mCherry (white). Western blots with anti-GFP antibodies detect the levels of Fluc^{DM}-EGFP, whereas Ponceau staining and α-tubulin are used as normalization controls. The toxic 49(GGGGCC) protein increases the detergent-insoluble levels of Fluc^{DM} variants that localize to the cytoplasm (A), mitochondria (B), and the nucleus (C), indicating that aggregation-prone proteins with 49(GGGGCC) repeats generally disrupt proteostasis across multiple cell compartments. $n = 3$ (biological replicates) with the mean ± SD indicated; $^{*}p < 0.05$, $^{**}p < 0.01$, $^{***}p < 0.001$ (one-way ANOVA).

(D–F) Western blots of detergent-soluble and -insoluble fractions from skeletal muscles of flies that express pathogenic ataxin-3 with poly-glutamine tract expansion (hATXN3.tr-Q78; red) versus a non-pathogenic ataxin-3 (hATXN3.tr-Q27, gray) and mCherry controls (white). There is no modulation of detergent-soluble and -insoluble Fluc^{DM} levels (D), whereas the effects of hATXN3.tr-Q78 on mito-Fluc^{DM} (E) and NLS-Fluc^{DM} (F) levels are inconsistent when compared to the hATXN3.tr-Q27 versus the mCherry control. $n = 3$ (biological replicates) with the mean ± SD indicated; $^{*}p < 0.05$, $^{**}p < 0.01$ (one-way ANOVA). Altogether, these findings indicate that distinct aggregation-prone proteins have strikingly different impacts on subcellular proteostasis.

tau.[7,89–93] For example, tau deranges nucleocytoplasmic transport[94] and nuclear architecture and chromatin organization,[95–97] and tau nuclear aggregates alter the composition and organization of nuclear speckles.[98] However, it remains largely unknown whether the effects of cytosolic tau on the nucleus and organelles derive from corresponding changes in the protein quality control of these cell compartments.

To address this question, we utilized knockin fly models[99,100] in which the endogenous *Drosophila* tau was substituted by pathogenic human tau^{V337}, which carries a mutation that causes frontotemporal dementia in humans.[101–103] Previous studies have shown that these knockin *Drosophila* models develop progressive signs of tauopathy during aging when heterozygous, including neurodegeneration and behavioral deficits in memory, locomotion, and sleep.[99,100] On this basis, we tested whether tau^{V337M} impacts the detergent-soluble and -insoluble levels of Fluc^{DM}, mito-Fluc^{DM}, and NLS-Fluc^{DM} compared to isogenic controls. For these studies, flies with ubiquitous expression of tau^{V337M} and of Fluc^{DM} variants were examined at 10, 30, and 60 days, which correspond to young, intermediate, and old

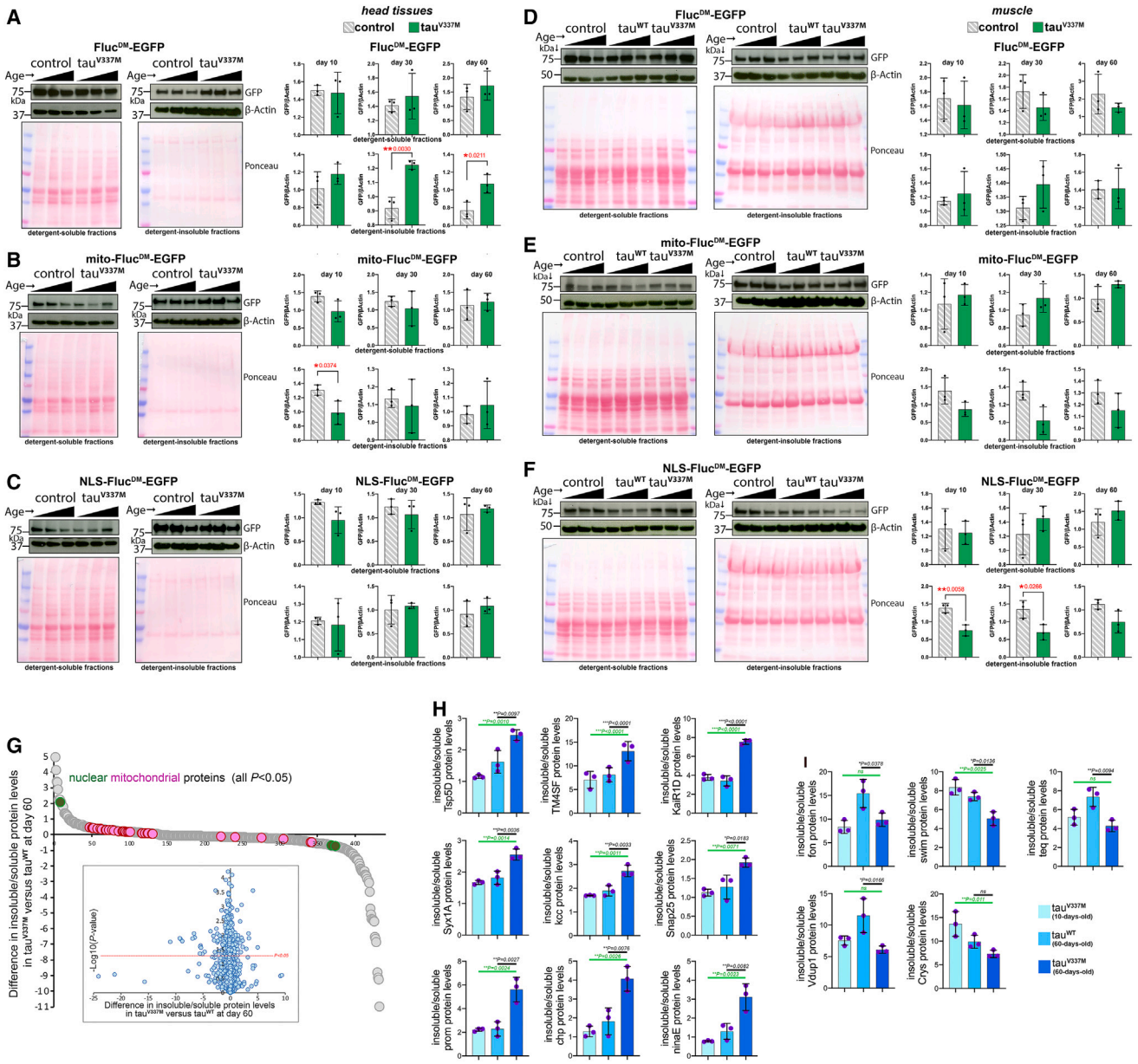

Figure 7. Pathogenic tau^{V337M} impacts subcellular proteostasis during aging in a contrasting manner

Western blots of detergent-soluble and -insoluble fractions from control flies (gray) and isogenic knockin flies that express human tau^{V337M} (green), a mutant tau that causes frontotemporal dementia in humans. Western blotting with anti-GFP antibodies indicates the levels of Fluc^{DM}-EGFP sensors, whereas Ponceau staining and β-actin are used as normalization controls.

(A–C) Analysis of detergent-soluble and -insoluble fractions from head extracts (enriched for tissues of the CNS) indicates that heterozygous tau^{V337M} mutations increase the detergent-insoluble levels of the cytoplasmic Fluc^{DM} reporter during aging (at 30 and 60 days) but not at a young age (10 days) compared to isogenic controls. There is little effect on the solubility of mito-Fluc^{DM} and NLS-Fluc^{DM}, indicating that tau^{V337M} reduces cytoplasmic proteostasis but has no substantial effect on mitochondrial and nuclear proteostasis in the CNS.

(D–F) Western blots of detergent-soluble and insoluble fractions from skeletal muscle (thoracic fractions) of flies with heterozygous tau^{V337M} mutations. There is no significant effect of pathogenic tau on Fluc^{DM} (D) and mito-Fluc^{DM} (E) levels, suggesting that the skeletal muscle may be resistant to tau^{V337M}-induced defects in cytoplasmic proteostasis (D) compared to the CNS (A). However, heterozygous tau^{V337M} mutations significantly reduce the detergent-insoluble levels of nuclearly localized NLS-Fluc^{DM} (F), suggesting that pathogenic tau^{V337M} may derange protein import into the nuclei of skeletal muscle.

In (A)–(F), the ages analyzed for each genotype are 10, 30, and 60 days. $n = 3$ (biological replicates) with the mean ± SD indicated; $^{*}p < 0.05$, $^{**}p < 0.01$ (unpaired two-tailed t test).

(G–I) Ultra-deep-coverage TMT mass spectrometry indicates that pathogenic tau^{V337M} divergently regulates the solubility of distinct protein sets. These proteomics analyses (18-plex TMT) are based on detergent-soluble and -insoluble fractions from isogenic knockin flies that express human tau^{WT} and pathogenic human tau^{V337M} at 10 and 60 days of age.

(legend continued on next page)

ages, and fly heads (enriched for the central nervous system) and thoraces (enriched for skeletal muscles) were analyzed separately.

Western blots of detergent-soluble and -insoluble fractions from fly heads revealed that, as expected, tau^{V337M} worsens cytosolic proteostasis, as indicated by a significant increase in the detergent-insoluble levels of the untargeted (~cytosolic) Fluc^{DM}, whereas its soluble levels were not affected (Figure 7A). Interestingly, these effects were significant at day 30 and day 60 but not at day 10 (Figure 7A), consistent with the previous finding that the development of tauopathy is progressive and age dependent in heterozygous tau^{V337M} flies.[99,100] There were minimal effects of tau^{V337M} on mitochondrial and nuclear proteostasis (Figures 7B and 7C), apart from a decrease in the insoluble mito-Fluc^{DM} levels at a young age (Figure 7B). Altogether, these analyses indicate that Fluc^{DM} insolubility is promoted by tau^{V337M} primarily in the cytoplasm and in an age-dependent manner.

Although pathogenic tau has been reported to impact skeletal muscle,[104–106] our analyses revealed minimal effects of pathogenic tau^{V337M} on cytosolic and mitochondrial proteostasis in this tissue, as assessed by monitoring the detergent-soluble and insoluble levels of the untargeted Fluc^{DM} (Figure 7D) and mito-Fluc^{DM} (Figure 7E) in muscle. Therefore, these findings suggest that skeletal muscle may be relatively resistant to derangement of cytoplasmic proteostasis by tau^{V337M} compared to the central nervous system. There was, however, an unexpected decline in the insoluble levels of NLS-Fluc^{DM} in response to tau^{V337M}, which may indicate derangement of nuclear protein import, whereas the soluble levels were unaffected (Figure 7F). Together, these findings indicate that pathogenic tau influences protein solubility in the nuclei of skeletal muscle cells (Figure 7F). Because such a reduction in insoluble NLS-Fluc^{DM} levels was not seen in fly head extracts (Figure 7C), which are enriched for the central nervous system, these findings suggest that the impact of pathogenic tau on subcellular proteostasis varies depending on the tissue and cell type.

Ultra-deep-coverage mass spectrometry indicates that pathogenic tau regulates, in opposite manners, the solubility of distinct protein sets during aging in *Drosophila*

To complement these analyses and determine how pathogenic tau impacts the solubility of the entire proteome, we next utilized ultra-deep-coverage tandem mass tag (TMT) mass spectrometry to analyze detergent-soluble and insoluble fractions. Also, in these studies, we utilized knockin tau models in which the endogenous *Drosophila* tau was replaced by wild-type human tau (tau^{WT}) or by pathogenic human tau^{V337M}.[99,100] On this basis, an 18-plex TMT analysis was done from whole flies with homozygous tau^{V337M} and control tau^{WT} expression at day 60, which corresponds to an old age in which behavioral deficits are manifest in tau^{V337M} versus tau^{WT} fly strains.[99,100] In addition, homozygous young (10-day-old) tau^{V337M} flies were examined to determine the age-related changes in protein solubility that occur with aging. This TMT-based profiling indicates that the solubility of several proteins is reshaped by tau^{V337M} compared to control, age-matched, isogenic tau^{WT} flies at 60 days of age (Figures 7G–7I; Table S2).

Because many proteins are expressed at the threshold of their solubility,[77,107–114] it has been hypothesized previously that aggregation-prone proteins generally tip the balance toward insolubility for other proteins. However, our TMT-based analyses indicate that pathogenic tau^{V337M} has complex effects on protein solubility: while some proteins become more insoluble, others display increased solubility upon expression of tau^{V337M} versus tau^{WT} (Figures 7G–7I, Figures S6A, and S6B).

We next examined the proteins with a significant difference ($p < 0.05$) in protein solubility (insoluble/soluble levels) in tau^{V337M} versus tau^{WT} flies to determine whether any specific subcellular compartment is impacted. While several mitochondrial proteins were among the proteins with solubility regulated by tau^{V337M} versus tau^{WT} (with primarily increased insolubility in response to tau^{V337M}), the magnitude of these changes, although significant ($p < 0.05$) was overall low (Figure 7G). Of the 3 significant proteins with nuclear localization, only one (nucleolar GTP-binding protein 1, CG8801) had increased insolubility in tau^{V337M} versus tau^{WT} (Figure 7G).

Further analysis of over-represented protein categories (Table S3) indicates that transmembrane proteins (e.g., tetraspanins), proteins with disordered domains, and proteins that are components of cell projections (e.g., axons) are enriched among proteins with tau^{V337M}-induced protein insolubility ($p < 0.05$ and $\Delta > 0.5$ for insoluble/soluble levels in tau^{V337M} versus tau^{WT}). Curated analyses further indicate the presence of several proteins involved in synaptic transmission and brain function (e.g., the kainate-type ionotropic glutamate receptor subunit 1D, the potassium:chloride symporter Kazachoc, axotactin, syntaxin-1A, adenylate cyclase, and synaptosomal-associated protein 25) and proteins enriched in microvilli and rhabdomeres and, hence, required for photoreceptor function (e.g., prominin, chaoptin, and opsin Rh1) (Figures 7H and S6C). Together, these findings suggest that tau^{V337M} may impact synaptic transmission[88,115–118] and light detection by photoreceptors (as reported for human patients and mouse models of tauopathy[119–123]) by perturbing the solubility of specific components of the synapse and of the light-sensing apparatus. Altogether, organism-wide profiling of proteome solubility indicates that tau^{V337M} particularly impacts the solubility of proteins involved in the function of the central nervous system. Conversely, proteins with tau^{V337M}-induced upregulation of solubility ($p < 0.05$ and $\Delta < -0.5$ for insoluble/soluble levels in tau^{V337M} versus tau^{WT})

(G) The difference in the insoluble/soluble protein levels in tau^{V337M} versus tau^{WT} at approximately day 60. There are 432 proteins of 4,012 quantified proteins that display significantly ($p < 0.05$) increased ($n = 140$; $n = 20$ with log2R > 1) and decreased ($n = 292$, $n = 43$ with log2R < −1) insolubility in tau^{V337M} versus tau^{WT} at day 60. These include mitochondrial (pink) and nuclear (green) proteins.

(H and I) Examples of proteins with increased (H) and decreased (I) insolubility in response to tau^{V337M} in old age compared to tau^{WT} at the same age (black line of comparison) and compared to tau^{V337M} at a young age (green line). $n = 3$ (biological replicates) with the mean ± SD indicated; $^{*}p < 0.05$, $^{**}p < 0.01$, $^{***}p < 0.001$ (one-way ANOVA).

are enriched in peptidases/proteases, glycoproteins, and proteins with disordered regions. Further refined analyses indicate that several secreted factors (e.g., Ance-3, Swim, teq, and fon) and the chaperone crystallin are among the proteins with improved solubility in tau^{V337M} versus control tau^{WT} flies (Figures 7I and S6C).

In summary, these proteomics analyses identify remarkably diverse impacts of pathogenic tau^{V337M} on protein solubility and also highlight subcellular compartments (cell projections and plasma membrane) that are particularly affected.

DISCUSSION

Eukaryotic cells have evolved complex functions via their compartmentalization into organelles and subcellular microenvironments.[124] Such specialization of the cellular space has enabled optimal organelle function but also resulted in compartment-specific challenges to proteostasis.[9,23,125] Consequently, organelle-specific stress responses and quality control mechanisms are in place to ensure proteostasis within each compartment.[2,18,19,126] Although the loss of proteostasis is a key hallmark of aging,[47] it remains largely unknown how subcellular proteostasis is impacted by environmental interventions and endocrine signaling factors that regulate aging. Moreover, while aggregation-prone proteins are the culprit of many age-related diseases,[7] it remains undetermined whether they perturb proteostasis across the cell or only in specific subcellular compartments.

In this study, we have generated *Drosophila* strains that ubiquitously express misfolding-prone Fluc^{DM} protein variants that were engineered to selectively localize to the nucleus and mitochondria, along with an untargeted variant that localizes primarily to the cytoplasm (Figure 1). By using these tools, we demonstrate that Fluc^{DM} protein variants can be utilized to perturb proteostasis in a compartment-targeted manner when compared to isogenic flies with no Fluc^{DM} expression. Analysis of the organism-wide consequences of these ubiquitous subcellular perturbations indicates that mild stress induced by expression of compartment-targeted Fluc^{DM} variants extends lifespan, impedes age-associated neuromuscular aging, and promotes proteostasis (Figure 2). At the molecular level, there are both common and variant-specific transcriptional responses that are induced by Fluc^{DM} (Figure 3). Apart from a strong induction of the mitochondrial small heat shock protein Hsp22 by all Fluc^{DM} variants, chaperones were not an overrepresented category among the differentially regulated genes (Figure 3B), suggesting that the transcriptional stress response induced by Fluc^{DM} variants is different from the heat shock response (HSR).[127,128] Likewise, apart from Hsp22, there was no upregulation of Hsp60 (Table S1; Figure S7), a mitochondrial chaperone that is stereotypically induced by the mitochondrial unfolded protein response (UPR^{mt}).[20,129] Altogether, these findings indicate that perturbation of subcellular proteostasis by Fluc^{DM} does not simply induce the HSR or the UPR^{mt} (Figure 3). Previous studies in cultured cells engineered to express nuclear and cytoplasmic proteins with destabilizing domains similarly found that the transcriptional stress response induced by these misfolding-prone proteins is distinct from the HSR and the UPR.[16] Altogether, these findings suggest that transcriptional responses different from the HSR and the UPR can be induced by misfolding-prone proteins targeted to specific subcellular compartments. Interestingly, Hsp22 levels have been identified previously as an important predictor of survival in *Drosophila* during aging,[35,45] indicating a possible role of this chaperone as part of the stress response and lifespan extension induced by Fluc^{DM} (Figure 2). However, apart from Hsp22, chaperones do not appear to be a major category of genes transcriptionally induced by Fluc^{DM} (Figure S7). Other gene categories were rather induced by Fluc^{DM}, including lipases and proteases, which may, respectively, help maintain metabolic homeostasis and protein quality control in cooperation with the ubiquitin-proteasome system and autophagy.[130]

In addition to utilizing Fluc^{DM} variants as tools to perturb subcellular proteostasis (Figures 2 and 3), we found that they can be used as reporters of proteostasis. Specifically, by measuring the detergent-soluble and insoluble levels of each Fluc^{DM}, the impact of genetic and environmental interventions on subcellular proteostasis can be determined compared to controls. In particular, the detergent insolubility of the untargeted Fluc^{DM}, mito-Fluc^{DM}, and NLS-Fluc^{DM} sensors increases to different degrees upon heat shock (Figure 4A). Moreover, the beneficial effects of cold shock may derive from an improvement in cytoplasmic proteostasis, as indicated by a reduction in the detergent-insoluble levels of the untargeted Fluc^{DM}, whereas mito-Fluc^{DM} and NLS-Fluc^{DM} were not affected (Figure 4B). Different endocrine signals that regulate aging (the glucagon-like hormone Akh[70–72] and Amyrel/maltose signaling[69]) also elicited remarkably distinct outcomes on subcellular proteostasis: while Akh improved nuclear proteostasis (by reducing the detergent-insoluble levels of NLS-Fluc^{DM}), Amyrel reduced the insoluble levels of the untargeted, largely cytoplasmic Fluc^{DM}. Because we induced Akh and Amyrel specifically in skeletal muscle and assessed the outcome systemically and/or in head extracts (which are enriched for the central nervous system), these findings suggest that endocrine signaling mediated by different muscle-secreted factors (myokines) may have remarkably distinct impacts on subcellular proteostasis. Physiologically, this may occur in response to muscle contraction because Amyrel is induced by cell stress,[69] which is a component of exercise,[131–135] and because glucagon-like peptide-1 (GLP-1, possibly related to Akh) is expressed by skeletal muscles in response to exercise in mice.[136] Altogether, these findings indicate that compartment-targeted Fluc^{DM} can be utilized as a sensor to determine whether environmental and genetic interventions regulate subcellular proteostasis.

We also examined how distinct aggregation-prone proteins impact the solubility of Fluc^{DM} sensors during aging. Aggregation-prone proteins can interact with and disrupt the folding status of other native proteins and impede proteasome activity.[7,23,74,76,125,137,138] On this basis, the toxicity of aggregation-prone proteins may derive from a widespread loss of protein quality control.[7,23,74,76,125,137,138] To test this hypothesis, here, we estimated the impact of different aggregation-prone proteins on the detergent-insoluble levels of compartment-targeted Fluc^{DM} reporters of proteostasis (Figures 6 and 7). Our analyses

indicate a range of diverse outcomes. A toxic protein with 49(GGGGCC) repeats, associated with amyotrophic lateral sclerosis and frontotemporal dementia,[80] widely impaired proteostasis across cell compartments (cytoplasm, mitochondria, and nucleus). Conversely, pathogenic ataxin-3 (hATXN3.tr-Q78) associated with Machado-Joseph disease/spinocerebellar ataxia[82] had minimal effects on the detergent-insoluble levels of all compartment-targeted Fluc^{DM} reporters (Figure 6).

In addition to 49(GGGGCC) and hATXN3.tr-Q78, we examined how a mutant form of MAPT[90,139] impacts Fluc^{DM} solubility. Normally, tau is predominantly (>90%) attached to microtubules, but its mutation and/or hyperphosphorylation promote its aggregation and accumulation into cytoplasmic neurofibrillary tangles in Alzheimer's disease and related dementias.[7,90,101,139,140] Recent evidence indicates that cytoplasmic, soluble oligomers of tau, generated during tangle formation, are the most toxic tau species that cause neurodegeneration.[7,89–91] Although the decline of proteostasis is a defining feature of tauopathies,[7,89–91] it remains largely undetermined whether cytoplasmic mutant tau regulates protein quality control in other cell compartments and organelles apart from the cytosol. By utilizing untargeted (~cytoplasmic) Fluc^{DM}, mito-Fluc^{DM}, and NLS-Fluc^{DM}, our analyses now indicate that pathogenic tau^{V337M} impairs proteostasis in the cytoplasm but not in the nucleus and mitochondria (Figures 7A–7C) and that this occurs in the central nervous system but not in the skeletal muscle (Figures 7D–7F). Therefore, although tau^{V337M} is known to derange the function of many cell compartments (e.g., mitochondria and the nucleus),[90,139] this does not seem to occur via a general perturbation of proteostasis in these compartments (as inferred from the detergent-insoluble levels of mito-Fluc^{DM} and NLS-Fluc^{DM}) but only in the cytoplasm.

In summary, our analyses indicate that the impact of aggregation-prone proteins on subcellular proteostasis is widely diverse: there is an overt decline in cytoplasmic, nuclear, and mitochondrial proteostasis in response to 49(GGGGCC) expression (Figure 6), whereas tau^{V337M} impedes only cytoplasmic protein quality control (Figure 7), and hATXN3.tr-Q78 has minimal impact (Figure 6). Altogether, these findings pinpoint that the toxicity of aggregation-prone proteins is not necessarily coupled to widespread disruption of proteostasis across cell compartments.

By analyzing the effects of pathogenic tau^{V337M} on subcellular proteostasis in head extracts (consisting mostly of tissues from the central nervous system, CNS) versus thoraces (consisting of skeletal muscle), we found that tau^{V337M} impedes cytoplasmic proteostasis in the CNS but not in muscle (Figure 7), consistent with the fact that tauopathies have primary manifestations in the brain and less so in peripheral tissues.[86–88] Interestingly, tau^{V337M} expression reduced the detergent-insoluble levels of NLS-Fluc^{DM} in muscle fractions (Figures 7D–7F), suggesting that pathogenic tau^{V337M} may derange nuclear protein import in muscle cells.

To further explore how tau^{V337M} impacts the solubility of the proteome, we utilized TMT mass spectrometry to profile the detergent-soluble and -insoluble levels of >4,000 proteins in whole flies that expressed endogenous levels of human tau^{V337M} compared to tau^{WT}. These analyses indicate that pathogenic tau^{V337M} does not simply skew the proteome toward insolubility but, rather, remodels protein solubility in a balanced manner: ~3.4% and ~7.2% of detected proteins displayed significantly increased and decreased insolubility, respectively, in tau^{V337M} versus tau^{WT} (Figures 7G–7I). While proteins with tau^{V337M}-modified solubility encompass several cell compartments, including the nucleus and mitochondria, there is an enrichment for transmembrane proteins and components of cell projections (e.g., axons). Functional categories of such proteins include synaptic function and light perception, suggesting that the solubility of proteins necessary for key functions of the CNS is prominently impacted by tau^{V337M}. These studies therefore indicate a complex remodeling of proteome solubility by pathogenic tau.

Altogether, transgenic *Drosophila* strains that express compartment-targeted Fluc^{DM} sensors provide tools to survey subcellular proteostasis and guide subsequent analyses. Depending on the experimental design, compartment-targeted Fluc^{DM} variants can be utilized as reporters or as tools to perturb subcellular proteostasis. On this basis, transgenic Fluc^{DM} strains may be utilized to determine how protein quality control is regulated across cell compartments during the progression of age-related diseases and by interventions that delay aging.

Limitations of the study

This study examined how Fluc^{DM}-based sensors of subcellular proteostasis can be utilized to either monitor or perturb subcellular proteostasis (depending on the experimental design) in the context of aging and age-associated conditions. To perturb subcellular proteostasis, Fluc^{DM} variants targeted to different subcellular compartments are compared to isogenic controls with no Fluc^{DM} to detect responses that are triggered by compartment-targeted Fluc^{DM}. However, we did not systematically examine the proteomic alterations resulting from Fluc^{DM} and how these compare to other established proteostatic challenges occurring during normal aging or experimental interventions. In a second application, Fluc^{DM} variants can be utilized to monitor the impact of an experimental intervention (genetic, pharmacologic, etc.) on subcellular proteostasis by comparing such interventions to controls that also express the same Fluc^{DM}. For this application, the measurement of luciferase activity does not appear to be a convenient readout for the mitochondrial and nuclear luciferases (mito-Fluc^{DM}-EGFP and NLS-Fluc^{DM}-EGFP) because of the low levels detected, which are presumably due to the low luciferase activity and/or low stability of these Fluc^{DM} variants. Because mitochondrial and nuclear proteins are translated in the cytoplasm and then imported into mitochondria and nuclei, the insolubility of mito-Fluc^{DM}-GFP and NLS-Fluc^{DM}-GFP may also reflect defects in protein import into these cellular compartments. Another limitation is that the Fluc^{DM} sensors indicate the general status of proteostasis but not necessarily that of individual proteins or specific protein categories. Our mass spectrometry data indeed indicate that pathogenic tau^{V337M} differentially remodels the solubility of distinct protein subsets (Figure 7).

RESOURCE AVAILABILITY

Lead contact

Requests for further information, resources, and reagents should be directed to and will be fulfilled by the lead contact, Fabio Demontis (Fabio.Demontis@stjude.org).

Materials availability

There are no restrictions on the availability of the data and tools generated by this study.

Data and code availability

- The data supporting the findings of this study are available within the paper (Figures 1, 2, 3, 4, 5, 6, 7 and S1–S7 and Tables S1–S5). The TMT mass spectrometry proteomics data have been deposited in the ProteomeXchange Consortium via the PRIDE partner repository and are accessible with the dataset identifier PRIDE: PXD045325. The RNA-seq data have been deposited in the Gene Expression Omnibus (GEO) with the identifier GEO: GSE243224.
- This paper does not report original code.
- Any other information required to reanalyze the data reported in this paper is available from the lead contact upon request.

ACKNOWLEDGMENTS

We thank Dr. Doris Kretzschmar for the tau knockin fly stocks and Dr. Ulrich Hartl for the pCI-FlucDM-EGFP plasmid. We also thank the Light Microscopy facility and the Hartwell Center for Bioinformatics and Biotechnology at St. Jude Children's Research Hospital and the Bloomington Drosophila stock center. Schematics were drawn with BioRender. This project was supported by the National Institute on Aging of the NIH (R21AG079267). The Demontis lab is also supported by the Alzheimer's Association (AARG-NTF-22-973220) and by the National Institute on Aging (R01AG075869). The Peng lab is supported by the NIH (RF1AG068581). The content is solely the responsibility of the authors and does not necessarily represent the official views of the National Institutes of Health. Research at St. Jude Children's Research Hospital is supported by ALSAC.

AUTHOR CONTRIBUTIONS

M.R. generated the Fluc^{DM} transgenic sensors. M.C. did most of the experiments with the Fluc^{DM} sensors together with M.R., C.-L.C., A.S., Z.C., and M.R.-M. V.P. did the TMT mass spectrometry and corresponding data analyses. Y.-D.W. analyzed the RNA-seq data. J.P. supervised the mass spectrometry studies. F.D. supervised the project and wrote the manuscript.

DECLARATION OF INTERESTS

The authors declare no competing interests.

STAR★METHODS

Detailed methods are provided in the online version of this paper and include the following:

- KEY RESOURCES TABLE
- EXPERIMENTAL MODEL AND SUBJECT DETAILS
  - *Drosophila* husbandry
- METHOD DETAILS
  - Drosophila stocks
  - Cloning and establishment of compartment-targeted Fluc^{DM} transgenic sensors in *Drosophila*
  - Immunostaining and laser scanning confocal microscopy of *Drosophila* tissues
  - RNA sequencing and hierarchical clustering
  - qRT-PCR
  - Analysis of aggregates of pathogenic huntingtin
  - Heat shock and cold shock
  - Western blots of detergent-soluble and insoluble protein fractions
  - Luciferase assays
  - Preparation of detergent-soluble and insoluble fractions, protein digestion, and peptide isobaric labeling by tandem mass tags
  - Two-dimensional HPLC and mass spectrometry
  - MS data analysis
- QUANTIFICATION AND STATISTICAL ANALYSIS

SUPPLEMENTAL INFORMATION

Supplemental information can be found online at https://doi.org/10.1016/j.crmeth.2024.100875.

Received: December 14, 2023
Revised: February 1, 2024
Accepted: September 12, 2024
Published: October 8, 2024

REFERENCES

1. Dillin, A., Gottschling, D.E., and Nyström, T. (2014). The good and the bad of being connected: the integrons of aging. Curr. Opin. Cell Biol. *26*, 107–112. https://doi.org/10.1016/j.ceb.2013.12.003.
2. Gottschling, D.E., and Nyström, T. (2017). The Upsides and Downsides of Organelle Interconnectivity. Cell *169*, 24–34. https://doi.org/10.1016/j.cell.2017.02.030.
3. Bouska, M., Huang, K., Kang, P., and Bai, H. (2019). Organelle aging: Lessons from model organisms. J Genet Genomics *46*, 171–185. https://doi.org/10.1016/j.jgg.2019.03.011.
4. Huang, K., Miao, T., Chang, K., Kim, J., Kang, P., Jiang, Q., Simmonds, A.J., Di Cara, F., and Bai, H. (2020). Impaired peroxisomal import in Drosophila oenocytes causes cardiac dysfunction by inducing upd3 as a peroxikine. Nat. Commun. *11*, 2943. https://doi.org/10.1038/s41467-020-16781-w.
5. Kim, J., and Bai, H. (2022). Peroxisomal Stress Response and Inter-Organelle Communication in Cellular Homeostasis and Aging. Antioxidants *11*, 192. https://doi.org/10.3390/antiox11020192.
6. DiLoreto, R., and Murphy, C.T. (2015). The cell biology of aging. Mol. Biol. Cell *26*, 4524–4531. https://doi.org/10.1091/mbc.E14-06-1084.
7. Douglas, P.M., and Dillin, A. (2010). Protein homeostasis and aging in neurodegeneration. J. Cell Biol. *190*, 719–729.
8. Demontis, F., Piccirillo, R., Goldberg, A.L., and Perrimon, N. (2013). Mechanisms of skeletal muscle aging: insights from Drosophila and mammalian models. Dis. Model. Mech. *6*, 1339–1352. https://doi.org/10.1242/dmm.012559.
9. Kirstein, J., Morito, D., Kakihana, T., Sugihara, M., Minnen, A., Hipp, M.S., Nussbaum-Krammer, C., Kasturi, P., Hartl, F.U., Nagata, K., and Morimoto, R.I. (2015). Proteotoxic stress and ageing triggers the loss of redox homeostasis across cellular compartments. EMBO J. *34*, 2334–2349. https://doi.org/10.15252/embj.201591711.
10. Gupta, R., Kasturi, P., Bracher, A., Loew, C., Zheng, M., Villella, A., Garza, D., Hartl, F.U., and Raychaudhuri, S. (2011). Firefly luciferase mutants as sensors of proteome stress. Nat. Methods *8*, 879–884. https://doi.org/10.1038/nmeth.1697.
11. Samant, R.S., Livingston, C.M., Sontag, E.M., and Frydman, J. (2018). Distinct proteostasis circuits cooperate in nuclear and cytoplasmic protein quality control. Nature *563*, 407–411. https://doi.org/10.1038/s41586-018-0678-x.
12. Henderson, K.A., Hughes, A.L., and Gottschling, D.E. (2014). Mother-daughter asymmetry of pH underlies aging and rejuvenation in yeast. Elife *3*, e03504. https://doi.org/10.7554/eLife.03504.
13. Veatch, J.R., McMurray, M.A., Nelson, Z.W., and Gottschling, D.E. (2009). Mitochondrial dysfunction leads to nuclear genome instability via an iron-sulfur cluster defect. Cell *137*, 1247–1258. https://doi.org/10.1016/j.cell.2009.04.014.
14. Peric, M., Bou Dib, P., Dennerlein, S., Musa, M., Rudan, M., Lovric, A., Nikolic, A., Saric, A., Sobocanec, S., Macak, Z., et al. (2016). Crosstalk between cellular compartments protects against proteotoxicity and extends lifespan. Sci. Rep. *6*, 28751. https://doi.org/10.1038/srep28751.

15. van Oosten-Hawle, P., Porter, R.S., and Morimoto, R.I. (2013). Regulation of organismal proteostasis by transcellular chaperone signaling. Cell *153*, 1366–1378. https://doi.org/10.1016/j.cell.2013.05.015.

16. Miyazaki, Y., Chen, L.C., Chu, B.W., Swigut, T., and Wandless, T.J. (2015). Distinct transcriptional responses elicited by unfolded nuclear or cytoplasmic protein in mammalian cells. Elife *4*, e07687. https://doi.org/10.7554/eLife.07687.

17. Shpilka, T., Du, Y., Yang, Q., Melber, A., Uma Naresh, N., Lavelle, J., Kim, S., Liu, P., Weidberg, H., Li, R., et al. (2021). UPR(mt) scales mitochondrial network expansion with protein synthesis via mitochondrial import in Caenorhabditis elegans. Nat. Commun. *12*, 479. https://doi.org/10.1038/s41467-020-20784-y.

18. Jovaisaite, V., Mouchiroud, L., and Auwerx, J. (2014). The mitochondrial unfolded protein response, a conserved stress response pathway with implications in health and disease. J. Exp. Biol. *217*, 137–143. https://doi.org/10.1242/jeb.090738.

19. Marciniak, S.J., and Ron, D. (2006). Endoplasmic reticulum stress signaling in disease. Physiol. Rev. *86*, 1133–1149.

20. Shpilka, T., and Haynes, C.M. (2018). The mitochondrial UPR: mechanisms, physiological functions and implications in ageing. Nat. Rev. Mol. Cell Biol. *19*, 109–120. https://doi.org/10.1038/nrm.2017.110.

21. Pakos-Zebrucka, K., Koryga, I., Mnich, K., Ljujic, M., Samali, A., and Gorman, A.M. (2016). The integrated stress response. EMBO Rep. *17*, 1374–1395. https://doi.org/10.15252/embr.201642195.

22. Blumenstock, S., Schulz-Trieglaff, E.K., Voelkl, K., Bolender, A.L., Lapios, P., Lindner, J., Hipp, M.S., Hartl, F.U., Klein, R., and Dudanova, I. (2021). Fluc-EGFP reporter mice reveal differential alterations of neuronal proteostasis in aging and disease. The EMBO journal *40*, e107260. https://doi.org/10.15252/embj.2020107260.

23. Labbadia, J., and Morimoto, R.I. (2015). The biology of proteostasis in aging and disease. Annu. Rev. Biochem. *84*, 435–464. https://doi.org/10.1146/annurev-biochem-060614-033955.

24. Cox, R.T., and Spradling, A.C. (2003). A Balbiani body and the fusome mediate mitochondrial inheritance during Drosophila oogenesis. Development *130*, 1579–1590.

25. Rizzuto, R., Brini, M., Pizzo, P., Murgia, M., and Pozzan, T. (1995). Chimeric green fluorescent protein as a tool for visualizing subcellular organelles in living cells. Curr. Biol. *5*, 635–642.

26. Lu, J., Wu, T., Zhang, B., Liu, S., Song, W., Qiao, J., and Ruan, H. (2021). Types of nuclear localization signals and mechanisms of protein import into the nucleus. Cell Commun. Signal. *19*, 60. https://doi.org/10.1186/s12964-021-00741-y.

27. Markstein, M., Pitsouli, C., Villalta, C., Celniker, S.E., and Perrimon, N. (2008). Exploiting position effects and the gypsy retrovirus insulator to engineer precisely expressed transgenes. Nat. Genet. *40*, 476–483.

28. Gargano, J.W., Martin, I., Bhandari, P., and Grotewiel, M.S. (2005). Rapid iterative negative geotaxis (RING): a new method for assessing age-related locomotor decline in Drosophila. Exp. Gerontol. *40*, 386–395.

29. Rhodenizer, D., Martin, I., Bhandari, P., Pletcher, S.D., and Grotewiel, M. (2008). Genetic and environmental factors impact age-related impairment of negative geotaxis in Drosophila by altering age-dependent climbing speed. Exp. Gerontol. *43*, 739–748.

30. Sujkowski, A., Bazzell, B., Carpenter, K., Arking, R., and Wessells, R.J. (2015). Endurance exercise and selective breeding for longevity extend Drosophila healthspan by overlapping mechanisms. Aging (Albany NY) *7*, 535–552. https://doi.org/10.18632/aging.100789.

31. Zhang, S., Binari, R., Zhou, R., and Perrimon, N. (2010). A genomewide RNA interference screen for modifiers of aggregates formation by mutant Huntingtin in Drosophila. Genetics *184*, 1165–1179. https://doi.org/10.1534/genetics.109.112516.

32. Hunt, L.C., Schadeberg, B., Stover, J., Haugen, B., Pagala, V., Wang, Y.D., Puglise, J., Barton, E.R., Peng, J., and Demontis, F. (2021). Antagonistic control of myofiber size and muscle protein quality control by the ubiquitin ligase UBR4 during aging. Nat. Commun. *12*, 1418. https://doi.org/10.1038/s41467-021-21738-8.

33. Jiao, J., Curley, M., Graca, F.A., Robles-Murguia, M., Shirinifard, A., Finkelstein, D., Xu, B., Fan, Y., and Demontis, F. (2023). Modulation of protease expression by the transcription factor Ptx1/PITX regulates protein quality control during aging. Cell Rep. *42*, 111970. https://doi.org/10.1016/j.celrep.2022.111970.

34. Xu, Z., Tito, A.J., Rui, Y.N., and Zhang, S. (2015). Studying polyglutamine diseases in Drosophila. Exp. Neurol. *274*, 25–41. https://doi.org/10.1016/j.expneurol.2015.08.002.

35. Morrow, G., Samson, M., Michaud, S., and Tanguay, R.M. (2004). Overexpression of the small mitochondrial Hsp22 extends Drosophila life span and increases resistance to oxidative stress. FASEB J *18*, 598–599. https://doi.org/10.1096/fj.03-0860fje.

36. Leuenberger, P., Ganscha, S., Kahraman, A., Cappelletti, V., Boersema, P.J., von Mering, C., Claassen, M., and Picotti, P. (2017). Cell-wide analysis of protein thermal unfolding reveals determinants of thermostability. Science *355*, eaai7825. https://doi.org/10.1126/science.aai7825.

37. Mateus, A., Määttä, T.A., and Savitski, M.M. (2016). Thermal proteome profiling: unbiased assessment of protein state through heat-induced stability changes. Proteome Sci. *15*, 13. https://doi.org/10.1186/s12953-017-0122-4.

38. Nguyen, V.T., Morange, M., and Bensaude, O. (1989). Protein denaturation during heat shock and related stress. Escherichia coli beta-galactosidase and Photinus pyralis luciferase inactivation in mouse cells. J. Biol. Chem. *264*, 10487–10492.

39. Lindquist, J.A., and Mertens, P.R. (2018). Cold shock proteins: from cellular mechanisms to pathophysiology and disease. Cell Commun. Signal. *16*, 63. https://doi.org/10.1186/s12964-018-0274-6.

40. Lee, H.J., Alirzayeva, H., Koyuncu, S., Rueber, A., Noormohammadi, A., and Vilchez, D. (2023). Cold temperature extends longevity and prevents disease-related protein aggregation through PA28gamma-induced proteasomes. Nat. Aging *3*, 546–566. https://doi.org/10.1038/s43587-023-00383-4.

41. Carvalho, G.B., Drago, I., Hoxha, S., Yamada, R., Mahneva, O., Bruce, K.D., Soto Obando, A., Conti, B., and Ja, W.W. (2017). The 4E-BP growth pathway regulates the effect of ambient temperature on Drosophila metabolism and lifespan. Proc. Natl. Acad. Sci. USA *114*, 9737–9742. https://doi.org/10.1073/pnas.1618994114.

42. Dudkevich, R., Koh, J.H., Beaudoin-Chabot, C., Celik, C., Lebenthal-Loinger, I., Karako-Lampert, S., Ahmad-Albukhari, S., Thibault, G., and Henis-Korenblit, S. (2022). Neuronal IRE-1 coordinates an organism-wide cold stress response by regulating fat metabolism. Cell Rep. *41*, 111739. https://doi.org/10.1016/j.celrep.2022.111739.

43. Al-Fageeh, M.B., and Smales, C.M. (2006). Control and regulation of the cellular responses to cold shock: the responses in yeast and mammalian systems. Biochem. J. *397*, 247–259. https://doi.org/10.1042/BJ20060166.

44. Saibil, H. (2013). Chaperone machines for protein folding, unfolding and disaggregation. Nat. Rev. Mol. Cell Biol. *14*, 630–642. https://doi.org/10.1038/nrm3658.

45. Yang, J., and Tower, J. (2009). Expression of hsp22 and hsp70 transgenes is partially predictive of drosophila survival under normal and stress conditions. J. Gerontol. A Biol. Sci. Med. Sci. *64*, 828–838. https://doi.org/10.1093/gerona/glp054.

46. Hartl, F.U., Bracher, A., and Hayer-Hartl, M. (2011). Molecular chaperones in protein folding and proteostasis. Nature *475*, 324–332. https://doi.org/10.1038/nature10317.

47. Lopez-Otin, C., Blasco, M.A., Partridge, L., Serrano, M., and Kroemer, G. (2013). The hallmarks of aging. Cell *153*, 1194–1217. https://doi.org/10.1016/j.cell.2013.05.039.

48. Lopez-Otin, C., Blasco, M.A., Partridge, L., Serrano, M., and Kroemer, G. (2022). Hallmarks of aging: An expanding universe. Cell *186*, 243–278. https://doi.org/10.1016/j.cell.2022.11.001.

49. Lopez-Otin, C., Galluzzi, L., Freije, J.M.P., Madeo, F., and Kroemer, G. (2016). Metabolic Control of Longevity. Cell *166*, 802–821. https://doi.org/10.1016/j.cell.2016.07.031.

50. Panowski, S.H., and Dillin, A. (2009). Signals of youth: endocrine regulation of aging in Caenorhabditis elegans. Trends Endocrinol. Metab. *20*, 259–264. https://doi.org/10.1016/j.tem.2009.03.006.

51. Droujinine, I.A., and Perrimon, N. (2016). Interorgan Communication Pathways in Physiology: Focus on Drosophila. Annu. Rev. Genet. *50*, 539–570. https://doi.org/10.1146/annurev-genet-121415-122024.

52. Neufer, P.D., Bamman, M.M., Muoio, D.M., Bouchard, C., Cooper, D.M., Goodpaster, B.H., Booth, F.W., Kohrt, W.M., Gerszten, R.E., Mattson, M.P., et al. (2015). Understanding the Cellular and Molecular Mechanisms of Physical Activity-Induced Health Benefits. Cell Metab. *22*, 4–11. https://doi.org/10.1016/j.cmet.2015.05.011.

53. Murphy, R.M., Watt, M.J., and Febbraio, M.A. (2020). Metabolic communication during exercise. Nat. Metab. *2*, 805–816. https://doi.org/10.1038/s42255-020-0258-x.

54. Russell, S.J., and Kahn, C.R. (2007). Endocrine regulation of ageing. Nat. Rev. Mol. Cell Biol. *8*, 681–691.

55. Jones, C.M., and Boelaert, K. (2015). The Endocrinology of Ageing: A Mini-Review. Gerontology *61*, 291–300. https://doi.org/10.1159/000367692.

56. Smith, H.J., Sharma, A., and Mair, W.B. (2020). Metabolic Communication and Healthy Aging: Where Should We Focus Our Energy? Dev. Cell *54*, 196–211. https://doi.org/10.1016/j.devcel.2020.06.011.

57. Antebi, A. (2004). Inside insulin signaling, communication is key to long life. Sci. Aging Knowledge Environ. *2004*, pe25.

58. Galluzzi, L., Yamazaki, T., and Kroemer, G. (2018). Linking cellular stress responses to systemic homeostasis. Nat. Rev. Mol. Cell Biol. *19*, 731–745. https://doi.org/10.1038/s41580-018-0068-0.

59. Rajan, A., and Perrimon, N. (2011). Drosophila as a model for interorgan communication: lessons from studies on energy homeostasis. Dev. Cell *21*, 29–31. https://doi.org/10.1016/j.devcel.2011.06.034.

60. Chow, L.S., Gerszten, R.E., Taylor, J.M., Pedersen, B.K., van Praag, H., Trappe, S., Febbraio, M.A., Galis, Z.S., Gao, Y., Haus, J.M., et al. (2022). Exerkines in health, resilience and disease. Nat. Rev. Endocrinol. *18*, 273–289. https://doi.org/10.1038/s41574-022-00641-2.

61. Demontis, F., Piccirillo, R., Goldberg, A.L., and Perrimon, N. (2013). The influence of skeletal muscle on systemic aging and lifespan. Aging Cell *12*, 943–949. https://doi.org/10.1111/acel.12126.

62. Gupta, R., Khan, R., and Cortes, C.J. (2021). Forgot to Exercise? Exercise Derived Circulating Myokines in Alzheimer's Disease: A Perspective. Front. Neurol. *12*, 649452. https://doi.org/10.3389/fneur.2021.649452.

63. Jiao, J., and Demontis, F. (2017). Skeletal muscle autophagy and its role in sarcopenia and organismal aging. Curr. Opin. Pharmacol. *34*, 1–6. https://doi.org/10.1016/j.coph.2017.03.009.

64. Pedersen, B.K. (2019). Physical activity and muscle-brain crosstalk. Nat. Rev. Endocrinol. *15*, 383–392. https://doi.org/10.1038/s41574-019-0174-x.

65. Pedersen, B.K., Akerström, T.C.A., Nielsen, A.R., and Fischer, C.P. (2007). Role of myokines in exercise and metabolism. J. Appl. Physiol. *103*, 1093–1098.

66. Pedersen, B.K., and Febbraio, M.A. (2008). Muscle as an endocrine organ: focus on muscle-derived interleukin-6. Physiol. Rev. *88*, 1379–1406.

67. Rai, M., and Demontis, F. (2016). Systemic Nutrient and Stress Signaling via Myokines and Myometabolites. Annu. Rev. Physiol. *78*, 85–107. https://doi.org/10.1146/annurev-physiol-021115-105305.

68. Rai, M., and Demontis, F. (2022). Muscle-to-Brain Signaling Via Myokines and Myometabolites. Brain Plast. *8*, 43–63. https://doi.org/10.3233/BPL-210133.

69. Rai, M., Coleman, Z., Curley, M., Nityanandam, A., Platt, A., Robles-Murguia, M., Jiao, J., Finkelstein, D., Wang, Y.D., Xu, B., et al. (2021). Proteasome stress in skeletal muscle mounts a long-range protective response that delays retinal and brain aging. Cell Metab. *33*, 1137–1154.e9. https://doi.org/10.1016/j.cmet.2021.03.005.

70. Post, S., Liao, S., Yamamoto, R., Veenstra, J.A., Nässel, D.R., and Tatar, M. (2019). Drosophila insulin-like peptide dilp1 increases lifespan and glucagon-like Akh expression epistatic to dilp2. Aging Cell *18*, e12863. https://doi.org/10.1111/acel.12863.

71. Katewa, S.D., Demontis, F., Kolipinski, M., Hubbard, A., Gill, M.S., Perrimon, N., Melov, S., and Kapahi, P. (2012). Intramyocellular fatty-acid metabolism plays a critical role in mediating responses to dietary restriction in Drosophila melanogaster. Cell Metab. *16*, 97–103. https://doi.org/10.1016/j.cmet.2012.06.005.

72. Waterson, M.J., Chung, B.Y., Harvanek, Z.M., Ostojic, I., Alcedo, J., and Pletcher, S.D. (2014). Water sensor ppk28 modulates Drosophila lifespan and physiology through AKH signaling. Proc. Natl. Acad. Sci. USA *111*, 8137–8142. https://doi.org/10.1073/pnas.1315461111.

73. Eisele, Y.S., Monteiro, C., Fearns, C., Encalada, S.E., Wiseman, R.L., Powers, E.T., and Kelly, J.W. (2015). Targeting protein aggregation for the treatment of degenerative diseases. Nat. Rev. Drug Discov. *14*, 759–780. https://doi.org/10.1038/nrd4593.

74. Klaips, C.L., Jayaraj, G.G., and Hartl, F.U. (2018). Pathways of cellular proteostasis in aging and disease. J. Cell Biol. *217*, 51–63. https://doi.org/10.1083/jcb.201709072.

75. Ross, C.A., and Poirier, M.A. (2004). Protein aggregation and neurodegenerative disease. Nat. Med. *10*, S10–S17.

76. Scior, A., Juenemann, K., and Kirstein, J. (2016). Cellular strategies to cope with protein aggregation. Essays Biochem. *60*, 153–161. https://doi.org/10.1042/EBC20160002.

77. Vendruscolo, M. (2012). Proteome folding and aggregation. Curr. Opin. Struct. Biol. *22*, 138–143. https://doi.org/10.1016/j.sbi.2012.01.005.

78. Wilson, D.M., 3rd, Cookson, M.R., Van Den Bosch, L., Zetterberg, H., Holtzman, D.M., and Dewachter, I. (2023). Hallmarks of neurodegenerative diseases. Cell *186*, 693–714. https://doi.org/10.1016/j.cell.2022.12.032.

79. Stamer, K., Vogel, R., Thies, E., Mandelkow, E., and Mandelkow, E.M. (2002). Tau blocks traffic of organelles, neurofilaments, and APP vesicles in neurons and enhances oxidative stress. J. Cell Biol. *156*, 1051–1063. https://doi.org/10.1083/jcb.200108057.

80. Goodman, L.D., Prudencio, M., Kramer, N.J., Martinez-Ramirez, L.F., Srinivasan, A.R., Lan, M., Parisi, M.J., Zhu, Y., Chew, J., Cook, C.N., et al. (2019). Toxic expanded GGGGCC repeat transcription is mediated by the PAF1 complex in C9orf72-associated FTD. Nat. Neurosci. *22*, 863–874. https://doi.org/10.1038/s41593-019-0396-1.

81. Frottin, F., Perez-Berlanga, M., Hartl, F.U., and Hipp, M.S. (2021). Multiple pathways of toxicity induced by C9orf72 dipeptide repeat aggregates and G(4)C(2) RNA in a cellular model. Elife *10*, e62718. https://doi.org/10.7554/eLife.62718.

82. Tsou, W.L., Burr, A.A., Ouyang, M., Blount, J.R., Scaglione, K.M., and Todi, S.V. (2013). Ubiquitination regulates the neuroprotective function of the deubiquitinase ataxin-3 in vivo. J. Biol. Chem. *288*, 34460–34469. https://doi.org/10.1074/jbc.M113.513903.

83. Raj, K., and Akundi, R.S. (2021). Mutant Ataxin-3-Containing Aggregates (MATAGGs) in Spinocerebellar Ataxia Type 3: Dynamics of the Disorder. Mol. Neurobiol. *58*, 3095–3118. https://doi.org/10.1007/s12035-021-02314-z.

84. Johnson, S.L., Ranxhi, B., Libohova, K., Tsou, W.L., and Todi, S.V. (2020). Ubiquitin-interacting motifs of ataxin-3 regulate its polyglutamine

toxicity through Hsc70-4-dependent aggregation. Elife *9*, e60742. https://doi.org/10.7554/eLife.60742.

85. Lee, D., Lee, Y.I., Lee, Y.S., and Lee, S.B. (2020). The Mechanisms of Nuclear Proteotoxicity in Polyglutamine Spinocerebellar Ataxias. Front. Neurosci. *14*, 489. https://doi.org/10.3389/fnins.2020.00489.
86. Wang, Y., and Mandelkow, E. (2016). Tau in physiology and pathology. Nat. Rev. Neurosci. *17*, 5–21. https://doi.org/10.1038/nrn.2015.1.
87. Strang, K.H., Golde, T.E., and Giasson, B.I. (2019). MAPT mutations, tauopathy, and mechanisms of neurodegeneration. Lab. Invest. *99*, 912–928. https://doi.org/10.1038/s41374-019-0197-x.
88. Ballatore, C., Lee, V.M.Y., and Trojanowski, J.Q. (2007). Tau-mediated neurodegeneration in Alzheimer's disease and related disorders. Nat. Rev. Neurosci. *8*, 663–672. https://doi.org/10.1038/nrn2194.
89. Cowan, C.M., and Mudher, A. (2013). Are tau aggregates toxic or protective in tauopathies? Front. Neurol. *4*, 114. https://doi.org/10.3389/fneur.2013.00114.
90. Polanco, J.C., Li, C., Bodea, L.G., Martinez-Marmol, R., Meunier, F.A., and Götz, J. (2018). Amyloid-beta and tau complexity - towards improved biomarkers and targeted therapies. Nat. Rev. Neurol. *14*, 22–39. https://doi.org/10.1038/nrneurol.2017.162.
91. Szabo, L., Eckert, A., and Grimm, A. (2020). Insights into Disease-Associated Tau Impact on Mitochondria. Int. J. Mol. Sci. *21*, 6344. https://doi.org/10.3390/ijms21176344.
92. Lasagna-Reeves, C.A., Castillo-Carranza, D.L., Sengupta, U., Clos, A.L., Jackson, G.R., and Kayed, R. (2011). Tau oligomers impair memory and induce synaptic and mitochondrial dysfunction in wild-type mice. Mol. Neurodegener. *6*, 39. https://doi.org/10.1186/1750-1326-6-39.
93. Shafiei, S.S., Guerrero-Muñoz, M.J., and Castillo-Carranza, D.L. (2017). Tau Oligomers: Cytotoxicity, Propagation, and Mitochondrial Damage. Front. Aging Neurosci. *9*, 83. https://doi.org/10.3389/fnagi.2017.00083.
94. Eftekharzadeh, B., Daigle, J.G., Kapinos, L.E., Coyne, A., Schiantarelli, J., Carlomagno, Y., Cook, C., Miller, S.J., Dujardin, S., Amaral, A.S., et al. (2018). Tau Protein Disrupts Nucleocytoplasmic Transport in Alzheimer's Disease. Neuron *99*, 925–940.e7. https://doi.org/10.1016/j.neuron.2018.07.039.
95. Cornelison, G.L., Levy, S.A., Jenson, T., and Frost, B. (2019). Tau-induced nuclear envelope invagination causes a toxic accumulation of mRNA in Drosophila. Aging Cell *18*, e12847. https://doi.org/10.1111/acel.12847.
96. Mahoney, R., Ochoa Thomas, E., Ramirez, P., Miller, H.E., Beckmann, A., Zuniga, G., Dobrowolski, R., and Frost, B. (2020). Pathogenic Tau Causes a Toxic Depletion of Nuclear Calcium. Cell Rep. *32*, 107900. https://doi.org/10.1016/j.celrep.2020.107900.
97. Frost, B., Hemberg, M., Lewis, J., and Feany, M.B. (2014). Tau promotes neurodegeneration through global chromatin relaxation. Nat. Neurosci. *17*, 357–366. https://doi.org/10.1038/nn.3639.
98. Lester, E., Ooi, F.K., Bakkar, N., Ayers, J., Woerman, A.L., Wheeler, J., Bowser, R., Carlson, G.A., Prusiner, S.B., and Parker, R. (2021). Tau aggregates are RNA-protein assemblies that mislocalize multiple nuclear speckle components. Neuron *109*, 1675–1691.e9. https://doi.org/10.1016/j.neuron.2021.03.026.
99. Cassar, M., Law, A.D., Chow, E.S., Giebultowicz, J.M., and Kretzschmar, D. (2020). Disease-Associated Mutant Tau Prevents Circadian Changes in the Cytoskeleton of Central Pacemaker Neurons. Front. Neurosci. *14*, 232. https://doi.org/10.3389/fnins.2020.00232.
100. Law, A.D., Cassar, M., Long, D.M., Chow, E.S., Giebultowicz, J.M., Venkataramanan, A., Strauss, R., and Kretzschmar, D. (2022). FTD-associated mutations in Tau result in a combination of dominant and recessive phenotypes. Neurobiol. Dis. *170*, 105770. https://doi.org/10.1016/j.nbd.2022.105770.
101. Gistelinck, M., Lambert, J.C., Callaerts, P., Dermaut, B., and Dourlen, P. (2012). Drosophila models of tauopathies: what have we learned? Int. J. Alzheimer's Dis. *2012*, 970980. https://doi.org/10.1155/2012/970980.
102. Spillantini, M.G., Crowther, R.A., Kamphorst, W., Heutink, P., and van Swieten, J.C. (1998). Tau pathology in two Dutch families with mutations in the microtubule-binding region of tau. Am. J. Pathol. *153*, 1359–1363. https://doi.org/10.1016/S0002-9440(10)65721-5.
103. Tanemura, K., Murayama, M., Akagi, T., Hashikawa, T., Tominaga, T., Ichikawa, M., Yamaguchi, H., and Takashima, A. (2002). Neurodegeneration with tau accumulation in a transgenic mouse expressing V337M human tau. J. Neurosci. *22*, 133–141.
104. Chen, X., Miller, N.M., Afghah, Z., and Geiger, J.D. (2019). Development of AD-Like Pathology in Skeletal Muscle. J. Parkinson's Dis. Alzheimer's Dis. *6*. https://doi.org/10.13188/2376-922x.1000028.
105. Kitazawa, M., Trinh, D.N., and LaFerla, F.M. (2008). Inflammation induces tau pathology in inclusion body myositis model via glycogen synthase kinase-3beta. Ann. Neurol. *64*, 15–24. https://doi.org/10.1002/ana.21325.
106. Wang, J., Gu, B.J., Masters, C.L., and Wang, Y.J. (2017). A systemic view of Alzheimer disease - insights from amyloid-beta metabolism beyond the brain. Nat. Rev. Neurol. *13*, 612–623. https://doi.org/10.1038/nrneurol.2017.111.
107. Ciryam, P., Antalek, M., Cid, F., Tartaglia, G.G., Dobson, C.M., Guettsches, A.K., Eggers, B., Vorgerd, M., Marcus, K., Kley, R.A., et al. (2019). A metastable subproteome underlies inclusion formation in muscle proteinopathies. Acta Neuropathol. Commun. *7*, 197. https://doi.org/10.1186/s40478-019-0853-9.
108. Ciryam, P., Kundra, R., Morimoto, R.I., Dobson, C.M., and Vendruscolo, M. (2015). Supersaturation is a major driving force for protein aggregation in neurodegenerative diseases. Trends Pharmacol. Sci. *36*, 72–77. https://doi.org/10.1016/j.tips.2014.12.004.
109. Ciryam, P., Tartaglia, G.G., Morimoto, R.I., Dobson, C.M., and Vendruscolo, M. (2013). Widespread aggregation and neurodegenerative diseases are associated with supersaturated proteins. Cell Rep. *5*, 781–790. https://doi.org/10.1016/j.celrep.2013.09.043.
110. Sui, X., Pires, D.E.V., Ormsby, A.R., Cox, D., Nie, S., Vecchi, G., Vendruscolo, M., Ascher, D.B., Reid, G.E., and Hatters, D.M. (2020). Widespread remodeling of proteome solubility in response to different protein homeostasis stresses. Proc. Natl. Acad. Sci. USA *117*, 2422–2431. https://doi.org/10.1073/pnas.1912897117.
111. Tartaglia, G.G., and Vendruscolo, M. (2009). Correlation between mRNA expression levels and protein aggregation propensities in subcellular localisations. Mol. Biosyst. *5*, 1873–1876. https://doi.org/10.1039/b913099n.
112. Vecchi, G., Sormanni, P., Mannini, B., Vandelli, A., Tartaglia, G.G., Dobson, C.M., Hartl, F.U., and Vendruscolo, M. (2020). Proteome-wide observation of the phenomenon of life on the edge of solubility. Proc. Natl. Acad. Sci. USA *117*, 1015–1020. https://doi.org/10.1073/pnas.1910444117.
113. Vendruscolo, M., Knowles, T.P.J., and Dobson, C.M. (2011). Protein solubility and protein homeostasis: a generic view of protein misfolding disorders. Cold Spring Harb. Perspect. Biol. *3*, a010454. https://doi.org/10.1101/cshperspect.a010454.
114. Walther, D.M., Kasturi, P., Zheng, M., Pinkert, S., Vecchi, G., Ciryam, P., Morimoto, R.I., Dobson, C.M., Vendruscolo, M., Mann, M., and Hartl, F.U. (2015). Widespread Proteome Remodeling and Aggregation in Aging C. elegans. Cell *161*, 919–932. https://doi.org/10.1016/j.cell.2015.03.032.
115. Sydow, A., Van der Jeugd, A., Zheng, F., Ahmed, T., Balschun, D., Petrova, O., Drexler, D., Zhou, L., Rune, G., Mandelkow, E., et al. (2011). Tau-induced defects in synaptic plasticity, learning, and memory are reversible in transgenic mice after switching off the toxic Tau mutant. J. Neurosci. *31*, 2511–2525. https://doi.org/10.1523/JNEUROSCI.5245-10.2011.
116. Wu, T.H., Lu, Y.N., Chuang, C.L., Wu, C.L., Chiang, A.S., Krantz, D.E., and Chang, H.Y. (2013). Loss of vesicular dopamine release precedes tauopathy in degenerative dopaminergic neurons in a Drosophila model

expressing human tau. Acta Neuropathol. *125*, 711–725. https://doi.org/10.1007/s00401-013-1105-x.

117. Yoshiyama, Y., Higuchi, M., Zhang, B., Huang, S.M., Iwata, N., Saido, T.C., Maeda, J., Suhara, T., Trojanowski, J.Q., and Lee, V.M.Y. (2007). Synapse loss and microglial activation precede tangles in a P301S tauopathy mouse model. Neuron *53*, 337–351. https://doi.org/10.1016/j.neuron.2007.01.010.

118. Mandelkow, E.M., and Mandelkow, E. (1998). Tau in Alzheimer's disease. Trends Cell Biol. *8*, 425–427. https://doi.org/10.1016/s0962-8924(98)01368-3.

119. Ashok, A., Singh, N., Chaudhary, S., Bellamkonda, V., Kritikos, A.E., Wise, A.S., Rana, N., McDonald, D., and Ayyagari, R. (2020). Retinal Degeneration and Alzheimer's Disease: An Evolving Link. Int. J. Mol. Sci. *21*, 7290. https://doi.org/10.3390/ijms21197290.

120. Chiasseu, M., Alarcon-Martinez, L., Belforte, N., Quintero, H., Dotigny, F., Destroismaisons, L., Vande Velde, C., Panayi, F., Louis, C., and Di Polo, A. (2017). Tau accumulation in the retina promotes early neuronal dysfunction and precedes brain pathology in a mouse model of Alzheimer's disease. Mol. Neurodegener. *12*, 58. https://doi.org/10.1186/s13024-017-0199-3.

121. Hart, N.J., Koronyo, Y., Black, K.L., and Koronyo-Hamaoui, M. (2016). Ocular indicators of Alzheimer's: exploring disease in the retina. Acta Neuropathol. *132*, 767–787. https://doi.org/10.1007/s00401-016-1613-6.

122. Ho, W.L., Leung, Y., Cheng, S.S.Y., Lok, C.K.M., Ho, Y.S., Baum, L., Yang, X., Chiu, K., and Chang, R.C.C. (2015). Investigating degeneration of the retina in young and aged tau P301L mice. Life Sci. *124*, 16–23. https://doi.org/10.1016/j.lfs.2014.12.019.

123. Lacomme, M., Hales, S.C., Brown, T.W., Stevanovic, K., Jolicoeur, C., Cai, J., Bois, T., Desrosiers, M., Dalkara, D., and Cayouette, M. (2022). Numb regulates Tau levels and prevents neurodegeneration in tauopathy mouse models. Sci. Adv. *8*, eabm4295. https://doi.org/10.1126/sciadv.abm4295.

124. Gabaldon, T. (2021). Origin and Early Evolution of the Eukaryotic Cell. Annu. Rev. Microbiol. *75*, 631–647. https://doi.org/10.1146/annurev-micro-090817-062213.

125. Morimoto, R.I., and Cuervo, A.M. (2014). Proteostasis and the aging proteome in health and disease. J. Gerontol. A Biol. Sci. Med. Sci. *69*, S33–S38. https://doi.org/10.1093/gerona/glu049.

126. Boulon, S., Westman, B.J., Hutten, S., Boisvert, F.M., and Lamond, A.I. (2010). The nucleolus under stress. Mol. Cell *40*, 216–227. https://doi.org/10.1016/j.molcel.2010.09.024.

127. Richter, K., Haslbeck, M., and Buchner, J. (2010). The heat shock response: life on the verge of death. Mol. Cell *40*, 253–266. https://doi.org/10.1016/j.molcel.2010.10.006.

128. Gomez-Pastor, R., Burchfiel, E.T., and Thiele, D.J. (2018). Regulation of heat shock transcription factors and their roles in physiology and disease. Nat. Rev. Mol. Cell Biol. *19*, 4–19. https://doi.org/10.1038/nrm.2017.73.

129. Owusu-Ansah, E., Song, W., and Perrimon, N. (2013). Muscle mitohormesis promotes longevity via systemic repression of insulin signaling. Cell *155*, 699–712. https://doi.org/10.1016/j.cell.2013.09.021.

130. Rai, M., Curley, M., Coleman, Z., and Demontis, F. (2022). Contribution of proteases to the hallmarks of aging and to age-related neurodegeneration. Aging Cell *21*, e13603. https://doi.org/10.1111/acel.13603.

131. Cordeiro, A.V., Peruca, G.F., Braga, R.R., Brícola, R.S., Lenhare, L., Silva, V.R.R., Anaruma, C.P., Katashima, C.K., Crisol, B.M., Barbosa, L.T., et al. (2021). High-intensity exercise training induces mitonuclear imbalance and activates the mitochondrial unfolded protein response in the skeletal muscle of aged mice. Geroscience *43*, 1513–1518. https://doi.org/10.1007/s11357-020-00246-5.

132. Wu, J., Ruas, J.L., Estall, J.L., Rasbach, K.A., Choi, J.H., Ye, L., Boström, P., Tyra, H.M., Crawford, R.W., Campbell, K.P., et al. (2011). The unfolded protein response mediates adaptation to exercise in skeletal muscle through a PGC-1alpha/ATF6alpha complex. Cell Metab. *13*, 160–169. https://doi.org/10.1016/j.cmet.2011.01.003.

133. Hart, C.R., Ryan, Z.C., Pfaffenbach, K.T., Dasari, S., Parvizi, M., Lalia, A.Z., and Lanza, I.R. (2019). Attenuated activation of the unfolded protein response following exercise in skeletal muscle of older adults. Aging (Albany NY) *11*, 7587–7604. https://doi.org/10.18632/aging.102273.

134. Hentila, J., Ahtiainen, J.P., Paulsen, G., Raastad, T., Hakkinen, K., Mero, A.A., and Hulmi, J.J. (2018). Autophagy is induced by resistance exercise in young men, but unfolded protein response is induced regardless of age. Acta Physiol. *224*, e13069. https://doi.org/10.1111/apha.13069.

135. Ogborn, D.I., McKay, B.R., Crane, J.D., Parise, G., and Tarnopolsky, M.A. (2014). The unfolded protein response is triggered following a single, unaccustomed resistance-exercise bout. Am. J. Physiol. Regul. Integr. Comp. Physiol. *307*, R664–R669. https://doi.org/10.1152/ajpregu.00511.2013.

136. Wu, L., Zhou, M., Li, T., Dong, N., Yi, L., Zhang, Q., and Mi, M. (2022). GLP-1 regulates exercise endurance and skeletal muscle remodeling via GLP-1R/AMPK pathway. Biochim. Biophys. Acta. Mol. Cell Res. *1869*, 119300. https://doi.org/10.1016/j.bbamcr.2022.119300.

137. Balch, W.E., Morimoto, R.I., Dillin, A., and Kelly, J.W. (2008). Adapting proteostasis for disease intervention. Science *319*, 916–919.

138. Hipp, M.S., Kasturi, P., and Hartl, F.U. (2019). The proteostasis network and its decline in ageing. Nat. Rev. Mol. Cell Biol. *20*, 421–435. https://doi.org/10.1038/s41580-019-0101-y.

139. Masters, C.L., Bateman, R., Blennow, K., Rowe, C.C., Sperling, R.A., and Cummings, J.L. (2015). Alzheimer's disease. Nat. Rev. Dis. Primers *1*, 15056. https://doi.org/10.1038/nrdp.2015.56.

140. Wegmann, S., Eftekharzadeh, B., Tepper, K., Zoltowska, K.M., Bennett, R.E., Dujardin, S., Laskowski, P.R., MacKenzie, D., Kamath, T., Commins, C., et al. (2018). Tau protein liquid-liquid phase separation can initiate tau aggregation. EMBO J. *37*, e98049. https://doi.org/10.15252/embj.201798049.

141. Demontis, F., Patel, V.K., Swindell, W.R., and Perrimon, N. (2014). Intertissue control of the nucleolus via a myokine-dependent longevity pathway. Cell Rep. *7*, 1481–1494. https://doi.org/10.1016/j.celrep.2014.05.001.

142. Demontis, F., and Perrimon, N. (2010). FOXO/4E-BP signaling in Drosophila muscles regulates organism-wide proteostasis during aging. Cell *143*, 813–825. https://doi.org/10.1016/j.cell.2010.10.007.

143. Hunt, L.C., and Demontis, F. (2022). Age-Related Increase in Lactate Dehydrogenase Activity in Skeletal Muscle Reduces Life Span in Drosophila. J. Gerontol. A Biol. Sci. Med. Sci. *77*, 259–267. https://doi.org/10.1093/gerona/glab260.

144. Hunt, L.C., Jiao, J., Wang, Y.D., Finkelstein, D., Rao, D., Curley, M., Robles-Murguia, M., Shirinifard, A., Pagala, V.R., Peng, J., et al. (2019). Circadian gene variants and the skeletal muscle circadian clock contribute to the evolutionary divergence in longevity across Drosophila populations. Genome Res. *29*, 1262–1276. https://doi.org/10.1101/gr.246884.118.

145. Keravala, A., and Calos, M.P. (2008). Site-specific chromosomal integration mediated by phiC31 integrase. Methods Mol. Biol. *435*, 165–173. https://doi.org/10.1007/978-1-59745-232-8_12.

146. Hunt, L.C., and Demontis, F. (2013). Whole-mount immunostaining of Drosophila skeletal muscle. Nat. Protoc. *8*, 2496–2501. https://doi.org/10.1038/nprot.2013.156.

147. Graca, F.A., Stephan, A., Wang, Y.D., Shirinifard, A., Jiao, J., Vogel, P., Labelle, M., and Demontis, F. (2023). Progressive development of melanoma-induced cachexia differentially impacts organ systems in mice. Cell Rep. *42*, 111934. https://doi.org/10.1016/j.celrep.2022.111934.

148. Graca, F.A., Rai, M., Hunt, L.C., Stephan, A., Wang, Y.-D., Gordon, B., Wang, R., Quarato, G., Xu, B., Fan, Y., et al. (2022). The myokine Fibcd1 is an endogenous determinant of myofiber size and mitigates

cancer-induced myofiber atrophy. Nat. Commun. *13*, 2370. https://doi.org/10.1038/s41467-022-30120-1.

149. Hunt, L.C., Pagala, V., Stephan, A., Xie, B., Kodali, K., Kavdia, K., Wang, Y.D., Shirinifard, A., Curley, M., Graca, F.A., et al. (2023). An adaptive stress response that confers cellular resilience to decreased ubiquitination. Nat. Commun. *14*, 7348. https://doi.org/10.1038/s41467-023-43262-7.

150. Huang, D.W., Sherman, B.T., Tan, Q., Collins, J.R., Alvord, W.G., Roayaei, J., Stephens, R., Baseler, M.W., Lane, H.C., and Lempicki, R.A. (2007). The DAVID Gene Functional Classification Tool: a novel biological module-centric algorithm to functionally analyze large gene lists. Genome Biol. *8*, R183. https://doi.org/10.1186/gb-2007-8-9-r183.

151. Rai, M., Curley, M., Coleman, Z., Nityanandam, A., Jiao, J., Graca, F.A., Hunt, L.C., and Demontis, F. (2021). Analysis of proteostasis during aging with western blot of detergent-soluble and insoluble protein fractions. STAR Protoc. *2*, 100628. https://doi.org/10.1016/j.xpro.2021.100628.

152. Robles-Murguia, M., Rao, D., Finkelstein, D., Xu, B., Fan, Y., and Demontis, F. (2020). Muscle-derived Dpp regulates feeding initiation via endocrine modulation of brain dopamine biosynthesis. Genes Dev. *34*, 37–52. https://doi.org/10.1101/gad.329110.119.

153. Jiao, J., Kavdia, K., Pagala, V., Palmer, L., Finkelstein, D., Fan, Y., Peng, J., and Demontis, F. (2021). An age-downregulated ribosomal RpS28 protein variant regulates the muscle proteome. G3 (Bethesda). G3 (Bethesda). *11*, jkab165. https://doi.org/10.1093/g3journal/jkab165.

154. Hunt, L.C., Stover, J., Haugen, B., Shaw, T.I., Li, Y., Pagala, V.R., Finkelstein, D., Barton, E.R., Fan, Y., Labelle, M., et al. (2019). A Key Role for the Ubiquitin Ligase UBR4 in Myofiber Hypertrophy in Drosophila and Mice. Cell Rep. *28*, 1268–1281.e6. https://doi.org/10.1016/j.celrep.2019.06.094.

155. Xu, P., Duong, D.M., and Peng, J. (2009). Systematical optimization of reverse-phase chromatography for shotgun proteomics. J. Proteome Res. *8*, 3944–3950. https://doi.org/10.1021/pr900251d.

156. Zaman, M., Fu, Y., Chen, P.C., Sun, H., Yang, S., Wu, Z., Wang, Z., Poudel, S., Serrano, G.E., Beach, T.G., et al. (2023). Dissecting Detergent-Insoluble Proteome in Alzheimer's Disease by TMTc-Corrected Quantitative Mass Spectrometry. Mol. Cell. Proteomics *22*, 100608. https://doi.org/10.1016/j.mcpro.2023.100608.

157. Bai, B., Tan, H., Pagala, V.R., High, A.A., Ichhaporia, V.P., Hendershot, L., and Peng, J. (2017). Deep Profiling of Proteome and Phosphoproteome by Isobaric Labeling, Extensive Liquid Chromatography, and Mass Spectrometry. Methods Enzymol. *585*, 377–395. https://doi.org/10.1016/bs.mie.2016.10.007.

158. Wang, X., Li, Y., Wu, Z., Wang, H., Tan, H., and Peng, J. (2014). JUMP: a tag-based database search tool for peptide identification with high sensitivity and accuracy. Mol. Cell. Proteomics *13*, 3663–3673. https://doi.org/10.1074/mcp.O114.039586.

159. Pagala, V.R., High, A.A., Wang, X., Tan, H., Kodali, K., Mishra, A., Kavdia, K., Xu, Y., Wu, Z., and Peng, J. (2015). Quantitative protein analysis by mass spectrometry. Methods Mol. Biol. *1278*, 281–305. https://doi.org/10.1007/978-1-4939-2425-7_17.

STAR★METHODS

KEY RESOURCES TABLE

REAGENT or RESOURCE	SOURCE	IDENTIFIER
Antibodies		
Rabbit anti-alpha-tubulin (11H10)	Cell Signaling Technologies	2125; RRID:AB_2619646
Rabbit anti-beta-actin	Cell Signaling Technologies	8457; RRID:AB_10950489
Rabbit anti-GFP	Cell Signaling Technologies	2956; RRID:AB_1196615
Anti-rabbit IgG, HRP-linked	Cell Signaling Technologies	7074; RRID:AB_2099233
Chicken anti-GFP	Aves	GFP-1010; RRID:AB_2307313
AlexaFluor488-conjugated anti-chicken	ThermoFisher	A-11039; RRID:AB_2534096
Mouse anti-ATP5a	Abcam	ab14748; RRID:AB_301447
AlexaFluor555-conjugated anti-mouse	LifeTechnologies	A28180; RRID:AB_2536164
Chemicals, peptides, and recombinant proteins		
Alexa Fluor 635 Phalloidin	LifeTechnologies	A22284
DAPI	ThermoFisher	D1306
SlowFade Gold antifade	Invitrogen	S36937
IQ Sybr Green supermix	Bio-Rad	170–8885
96-well PCR plates	Bio-Rad	HSP9601
PBS	Gibco	10010023
Blue loading buffer pack	Cell Signaling Technologies	7722
Precision Plus protein standard	Bio-Rad	1610374
4–20% Mini-PROTEAN TGX pre-cast gels	Bio-Rad	4561096
Immobilon-P PVDF membrane	Millipore	IPVH00010
Ponceau S	ThermoFisher	A40000279
16% Paraformaldehyde	Electron Microscopy Sciences	15710
NP40 cell lysis buffer	Invitrogen	FNN0021
TRIzol	Ambion	15596018
Critical commercial assays		
Pierce BCA protein assay kit	ThermoScientific	23225
Dual-Glo luciferase assay system	Promega	E2920
iScript reverse transcriptase	Bio-Rad	1708840
Deposited data		
TMT mass spectrometry proteomics data of solubility changes induced by tau	This study	ProteomeXchange Consortium, PRIDE: PXD045325
RNA-seq data of gene expression changes induced by $Fluc^{DM}$	This study	Gene Expression Omnibus, GEO: GSE243224
Experimental models: Organisms/strains		
Drosophila: Mhc-Gal4	Demontis lab collection	Demontis et al., 2014[141]
Drosophila: GMR-Gal4	Demontis lab collection	Jiao et al., 2023[33]
Drosophila: UAS-mCherry	Bloomington stock center	#35787
Drosophila: UAS-8(GGGGCC)	Bloomington stock center	#84724
Drosophila: UAS-49(GGGGCC)	Bloomington stock center	#84727
Drosophila: UAS-hATXN3.tr-Q27	Bloomington stock center	#8149
Drosophila: UAS-Htt-Q72-GFP	Gift of Dr. Sheng Zhang	Zhang et al., 2010[31]
Drosophila: knock-in tau^{V337M}	Gift of Dr. Doris Kretzschmar	Cassar et al., 2020[99]
Drosophila: knock-in tau^{WT}	Gift of Dr. Doris Kretzschmar	Cassar et al., 2020[99]

(*Continued on next page*)

Continued

REAGENT or RESOURCE	SOURCE	IDENTIFIER
Drosophila: UAS-mCherry^{RNAi}	Bloomington stock center	#35785
Drosophila: UAS-Hsp70^{RNAi}	Bloomington stock center	#33948
Drosophila: UAS-Hsp22	Bloomington stock center	#20055
Drosophila: UAS-Akh	Bloomington stock center	#27343
Drosophila: UAS-Amyrel	Demontis lab collection	Rai et al., 2021[69]
Drosophila: tubulin_Fluc^{DM}-EGFP	This study	N/A
Drosophila: tubulin_mito-Fluc^{DM}-EGFP	This study	N/A
Drosophila: tubulin_NLS-Fluc^{DM}-EGFP	This study	N/A
Oligonucleotides		
Primers: *Hsp22* forward: 5′-CTTACCGATGTTTTGGCGCA-3′	This study	N/A
Primers: *Hsp22* reverse: 5′-TCGTGGAAGAAGGCGTGAAA-3′	This study	N/A
Primers: *Hsp70Bb* forward: 5′-AAATCGGATGGAGAGTTGGC-3′	This study	N/A
Primers: *Hsp70Bb* reverse: 5′-TGTAGGCGGGTTTTTGTTT-3′	This study	N/A
Primers: *Akh* forward: 5′-AAGCACCGCGAGTAGATAGC-3′	This study	N/A
Primers: *Akh* reverse: 5′-TGTGTGTGCGTGCTAGACAT-3′	This study	N/A
Primers: *Tub84B* forward: 5′-GCTGTTCCACCCCGAGCAGCTGATC-3′	This study	N/A
Primers: *Tub84B* reverse: 5′-GGCGAACTCCAGCTTGGACTTCTTGC-3′	This study	N/A
Primers: *Fluc (firefly luciferase)* forward: 5′-CCCTGGTTCCTGGAACAATTGC-3′	This study	N/A
Primers: *Fluc (firefly luciferase)* reverse: 5′-AAGAATTGAAGAGAGTTTTCACTGC-3′	This study	N/A
Software and algorithms		
Cell Profiler 3.0.0	Cell Profiler	https://www.cellprofiler.org
GraphPad Prism	GraphPad Prism	https://www.graphpad.com/
Photoshop 2023	Adobe	https://www.adobe.com/products/photoshop.html
Excel	Microsoft	https://www.microsoft.com
BioRender	BioRender	https://www.biorender.com

EXPERIMENTAL MODEL AND SUBJECT DETAILS

Drosophila husbandry

Flies were kept (~30 flies/tube) at 25°C, 60% humidity, and a 12h/12h light-dark cycle in tubes containing cornmeal/soy flour/yeast fly food. The fly food was changed regularly every 2–3 days. Flies were aged to 10, 30, and 60 days at 25°C (unless otherwise indicated). Similar procedures as previously reported were utilized for measuring survival during aging and for negative geotaxis.[141–144] All experiments were done with male flies.

METHOD DETAILS

Drosophila stocks

The following fly stocks were utilized in this study: *Mhc-Gal4*,[141–144] *GMR-Gal4*,[33] *UAS-mCherry* (Bloomington stock center #35787), *UAS-8(GGGGCC)* repeats (non-toxic control; #84724), *UAS-49(GGGGCC)* repeats (toxic poly-GA proteins, as found in C9orf72 associated with ALS and FTD; #84727),[80] *UAS-hATXN3.tr-Q27* (non-toxic control; #8149), *UAS-hATXN3.tr-Q78* (expresses a toxic C-terminal fragment of the human Machado-Joseph Disease/Spinocerebellar Ataxia 3 protein with a 78 repeat polyglutamine tract; #8150), *UAS-Htt-Q72-GFP*,[31–33] and knock-in tau models in which the endogenous *Drosophila* tau has been replaced by wild-type

human tau (tau^{WT}) and by pathogenic human tau^{V337M}.[99,100] These additional fly stocks were also utilized: *UAS-mCherry^{RNAi}* (#35785), *UAS-Hsp70^{RNAi}* (#33948), and *UAS-Hsp22* (#20055). Fluc^{DM} stocks (generated as indicated below), *UAS-Akh* (#27343), and *UAS-Amyrel*[69] were backcrossed against the *w^{1118}* background and compared to their respective litter-mate isogenic controls with no transgene expression.

Cloning and establishment of compartment-targeted Fluc^{DM} transgenic sensors in *Drosophila*

A *pCaSpeR5-attB-tubulin promoter* vector was generated by PCR-mediated amplification and cloning of a *tubulin* promoter and *attB* sequences by using *Kpn*I with *EcoR*I-HF, and *EcoR*I-HF, respectively. To express a general, untargeted version of a misfolding-prone luciferase (Fluc^{DM}),[10] Fluc^{DM} fused with EGFP was PCR-amplified from the *pCI-Fluc^{DM}-EGFP* plasmid[10] and cloned into the *pCaSpeR5-attB-tubulin promoter* vector with *Kpn*I-HF and *Xba*I. A similar procedure was used to clone a mitochondrially-targeted version of Fluc^{DM}-EGFP (mito-Fluc^{DM}), which consists of a mitochondrial target sequence from human COX VIII (MRLRLTVFCGVLRAIMSVLTPLLLRGLTGSARRLPVPRAK, previously utilized for establishing the mito-GFP *Drosophila* stock, Bloomington #8442),[24,25] a linker (RSS), and Fluc^{DM}-EGFP. For establishing Fluc^{DM} targeted to the nucleus (NLS-Fluc^{DM}), the canonical PAAKRVKLD nuclear localization signal[26] was added by PCR to the N-terminus of Fluc^{DM}-EGFP. These plasmids were injected into *w^{1118};attP40* embryos and *tubulin-Fluc^{DM}-EGFP* transgenic *Drosophila* stocks were established by phiC31-mediated site integration.[145]

Immunostaining and laser scanning confocal microscopy of *Drosophila* tissues

Drosophila brains and guts from Fluc^{DM} transgenic stocks, established as described above, were immunostained according to standard procedures.[32,144,146] Specifically, brains and guts were dissected and immediately fixed with 4% paraformaldehyde and 0.2% Triton X-100 for 30 min, washed, and then incubated with 1:200 chicken anti-GFP (Aves #GFP-1010) primary antibodies, followed by AlexaFluor488-conjugated anti-chicken secondary antibodies (ThermoFisher #A11039) together with DAPI (ThermoFisher #D1306) and AlexaFluor635-conjugated phalloidin (Life Technologies #A22284). Co-staining with mouse anti-ATP5a (abcam #14748) was done to assess the degree of mito-Fluc^{DM} localization to mitochondria, identified by the mitochondrial marker ATP5a. The samples were mounted on glass slides with SlowFade Gold antifade reagent (Invitrogen #S36937) and #1.5 coverslips and imaged by using a Zeiss LSM780 confocal microscope. Enterocytes of the midgut and brain cells of the antennal lobes are shown in the representative images in Figures 1B–1D.

RNA sequencing and hierarchical clustering

Samples for RNA sequencing were prepared with TRIzol (Ambion #15596018) from whole flies and the RNA was extracted by isopropanol precipitation from the aqueous phase.[147–149] RNA sequencing libraries for each sample were prepared from 1 μg total RNA by using the Illumina TruSeq RNA Sample Prep v2 Kit per the manufacturer's instructions, and sequencing was completed on the Illumina NovaSeq 6000. The 100-bp paired-end reads were trimmed, filtered against quality (Phred-like Q20 or greater) and length (50-bp or longer), and aligned to the Drosophila melanogaster reference genome (BDGP6/dm6) by using CLC Genomics Workbench v12.0.1 (Qiagen). For gene expression comparisons, we obtained the TPM (transcripts per million) counts from the CLC RNA-Seq Analysis tool. The differential gene expression analysis was performed by applying the non-parametric ANOVA using Kruskal-Wallis and Dunn's tests on log-transformed TPM, implemented in the Partek Genomics Suite v7.0 software (Partek Inc.). Hierarchical clustering of RNA-seq data into heatmaps was done by using the UPGMA clustering method (unweighted pair group method with arithmetic mean) with similarity measure of correlation, implemented in Spotfire v7.5.0 software (TIBCO). The RNA-seq data discussed in this publication are available in Table S1 and have been deposited in the NCBI's Gene Expression Omnibus (GEO) with accession number GEO: GSE243224. GO terms analysis was done with DAVID.[150]

qRT-PCR

For qRT-PCR, cDNAs were reverse transcribed with the iScript cDNA synthesis kit (Bio-Rad #1708840) from 1 μg total RNA. qRT-PCR was performed by using the IQ Sybr Green supermix (Bio-Rad #170–8885). *Tub84B* was utilized as normalization. The following qRT-PCR oligos were used:

Hsp22: 5′-CTTACCGATGTTTTGGCGCA-3′ and 5′-TCGTGGAAGAAGGCGTGAAA-3'
Hsp70Bb: 5′-AAATCGGATGGAGAGTTGGC-3′ and 5′-TGTAGGCGGGTTTTTGTTT-3'
Akh: 5′-AAGCACCGCGAGTAGATAGC-3′ and 5′-TGTGTGTGCGTGCTAGACAT-3'
Tub84B: 5′-GCTGTTCCACCCCGAGCAGCTGATC-3′ and 5′-GGCGAACTCCAGCTTGGACTTCTTGC-3'
Fluc (firefly luciferase): 5′-CCCTGGTTCCTGGAACAATTGC-3′ and 5′-AAGAATTGAAGAGAGTTTTCACTGC-3'

Analysis of aggregates of pathogenic huntingtin

Pathogenic huntingtin-polyQ72-GFP protein aggregates were imaged as previously done[33] by using a ZEISS SteREO Discovery.V12 epifluorescence microscope. Subsequently, the images were analyzed using Cell Profiler 3.0.0 (cellprofiler.org) to quantify the total area of protein aggregates (Huntingtin-polyQ72-GFP speckles) normalized by the retinal tissue area. This analysis was done with male flies after aging them at 25°C for 30 days.

Heat shock and cold shock

For the analysis of Fluc^{DM} solubility upon thermal stress, 14-days-old wild-type flies were heat shocked at 36°C for 3 h. For cold shock, 14-days-old flies were housed at 4°C for 2 h. Only flies that were alive after the heat and cold shocks were utilized for subsequent analyses.

Western blots of detergent-soluble and insoluble protein fractions

Western blots of detergent-soluble and insoluble fractions were obtained substantially as described previously.[142,151] Specifically, whole bodies, heads, or thoraces were homogenized in 60 μL ice-cold Triton X-100 buffer (1% Triton X-100 in PBS containing protease inhibitors and phosphatase inhibitors) for 5 min at the highest speed. Homogenates were centrifuged at 14,000 rpm at 4°C for 10 min and the supernatant was collected (Triton X-100 soluble fraction). The remaining pellet was washed in 400 μL Triton X-100 buffer and centrifuged twice at 14,000 rpm for 5 min at 4°C. The pellet was then resuspended at room temperature in 60 μL RIPA buffer containing 8M urea and 5% SDS, centrifuged at 14,000 rpm at 4°C for 10 min, and the supernatant collected (Triton X-100 insoluble fraction). 8 μL of soluble/insoluble protein extracts were boiled with sample buffer containing DTT and used for SDS-PAGE. Detergent-soluble and insoluble fractions were analyzed on 4–20% SDS-PAGE with anti-GFP antibodies (1:500, dissolved in TBST; Cell Signaling Technologies, #2956). Ponceau S staining (ThermoFisher #A40000279) and anti-β-actin and/or anti-α-tubulin antibodies (Cell Signaling Technologies, #8457 and #2125) were used as loading controls. The western blots with head samples were typically normalized by β-actin whereas the blots with thoracic samples were normalized by Ponceau staining or α-tubulin.

Luciferase assays

For luciferase assays, 10 thoraces/replicate were homogenized in 170 μL ice-cold homogenization buffer (250 mM sucrose, 50 mM Tris-HCl, 5 mM $MgCl_2$, and protease inhibitors) in a NextAdvance bullet blender at 4°C. Subsequently, 90 μL of the homogenate was transferred to a new tube and gently mixed with an equal volume of Dual-Glo luciferase reagent (Promega).[141,142,152] After a 10-min incubation, the luminescence was read with a Tecan Infinite 200 Pro. Luciferase readings were normalized by the protein content, as estimated with the Pierce BCA protein assay kit (Thermo Scientific).

Preparation of detergent-soluble and insoluble fractions, protein digestion, and peptide isobaric labeling by tandem mass tags

For TMT of *Drosophila* samples, 25 male flies per sample (n = 3 biological replicates per condition) were collected at day 10 and day ~60 from eclosion and homogenized in 200 μL NP40 cell lysis buffer (Invitrogen #FNN0021) with protease and phosphatase inhibitors and 0.5-mm zirconium beads in a NextAdvance bullet blender.[153,154] After homogenization, the samples were centrifuged at maximum speed for 10 min, and the supernatant was collected (corresponding to the detergent-soluble fraction, typically consisting of >100 μg). The remaining pellet was washed 3x in PBS and homogenized in insoluble lysis buffer containing 8M urea, PBS, and 1% SDS (with protease and phosphatase inhibitors). The resulting supernatant was collected (corresponding to the detergent-insoluble fraction, typically consisting of >10 μg). All the samples were then prepared for subsequent analyses by adding SDS-blue loading buffer and DTT (Cell Signaling Technologies #7722), and by heating them for 5 min at 95°C. The protein concentration of the lysates was determined by Coomassie-stained short gels using bovine serum albumin (BSA) as standard.[155] Specifically, the samples were run on 7.5% SDS-page gels at 60V for 10–15 min, or until all the protein was through the initial lane. BSA was used as a standard at 0.2, 1, and 5 mg. The gels were washed in distilled water and stained with Coomassie blue for 1–4 h with gentle shaking at room temperature, shielded from light. The gels were then de-stained with distilled water overnight at 4°C with gentle shaking. The bands were excised from the gels, cut into several pieces, collected into 1.5 mL-eppendorf tubes on ice, and stored at −80°C.

In preparation for TMT,[156] the short gel bands were washed twice with 50% acetonitrile and dried. The dried gel bands were then incubated with trypsin at an enzyme-to-substrate ratio of 1:10 (w/w) for overnight digestion. Following the overnight digestion, the peptide solution from the short gel bands was extracted, and the peptides were reduced by adding 1 mM DTT for 30 min at room temperature followed by alkylation with 10 mM iodoacetamide (IAA) for 30 min in the dark at room temperature. The unreacted IAA was quenched with 30 mM DTT for 30 min. Finally, the digestion was terminated and acidified by adding trifluoroacetic acid (TFA) to 1%, desalted using C18 cartridges (Harvard Apparatus), and dried by speed vac. The peptide mixture was resuspended in 50 mM HEPES (pH 8.5) and labeled with 18-plex Tandem Mass Tag (TMT) reagents (ThermoScientific) following the manufacturer's recommendations.

Two-dimensional HPLC and mass spectrometry

The TMT-labeled samples were mixed equally, desalted, and fractionated on an offline HPLC (Agilent 1220) using basic pH reverse-phase liquid chromatography (pH 8.0, XBridge C18 column, 4.6 mm × 25 cm, 3.5 μm particle size, Waters). The fractions were dried and resuspended in 5% formic acid and analyzed by acidic pH reverse phase LC-MS/MS analysis. The peptide samples were loaded on a nanoscale capillary reverse phase C18 column (New objective, 75 μm ID × ~25 cm, 1.9 μm C18 resin from Dr. Maisch GmbH) by an HPLC system (Thermo Ultimate 3000) and eluted by a 60-min gradient. The eluted peptides were ionized by electrospray ionization and detected by an inline Orbitrap Fusion mass spectrometer (ThermoScientific). The mass spectrometer is operated in data-dependent mode with a survey scan in Orbitrap (60,000 resolution, 1×10^6 AGC target and 50 m maximal ion time) and MS/MS high-resolution scans (60,000 resolution, 2×10^5 AGC target, 120 m maximal ion time, 32 HCD normalized collision energy, 1 m/z isolation window, and 15 s dynamic exclusion).[157]

MS data analysis

The MS/MS raw files were processed by the tag-based hybrid search engine JUMP.[158] The raw data were searched against the UniProt *Drosophila* database concatenated with a reversed decoy database for evaluating false discovery rates. Searches were performed using a 15-ppm mass tolerance for both precursor and product ions, fully tryptic restriction with two maximal missed cleavages, three maximal modification sites, and the assignment of *a*, *b*, and *y* ions. TMT tags on Lys and N-termini (+304.20715 Da) were used for static modifications and Met oxidation (+15.99492 Da) was considered as a dynamic modification. Matched MS/MS spectra were filtered by mass accuracy and matching scores to reduce the protein false discovery rate to ~1%. Proteins were quantified by summing reporter ion intensities across all matched PSMs using the JUMP software suite.[159] Categories enriched in protein sets were identified with DAVID.[150]

The TMT mass spectrometry proteomics data are reported in Table S2 and have been deposited to the ProteomeXchange Consortium via the PRIDE partner repository with the dataset identifier PRIDE: PXD045325.

QUANTIFICATION AND STATISTICAL ANALYSIS

Data organization, scientific graphing, and statistical analyses were done with Microsoft Excel (version 14.7.3) and GraphPad Prism (version 8). The unpaired two-tailed Student's t test was used to compare the means of two independent groups to each other. One-way ANOVA was used for multiple comparisons of more than two groups of normally distributed data. Survival and climbing data were analyzed with the log-rank test. The n for each experiment can be found in the figures and represents independently generated samples. Bar graphs represent the mean ± SD or the mean ± SEM, as specified in the figure legend. A significant result was defined as $p < 0.05$. Throughout the figures, asterisks indicate the significance of p values: $^{*}p < 0.05$, $^{**}p < 0.01$, and $^{***}p < 0.001$.

Cell Reports Methods, Volume *4*

Supplemental information

Transgenic sensors reveal compartment-specific effects of aggregation-prone proteins on subcellular proteostasis during aging

Michelle Curley, Mamta Rai, Chia-Lung Chuang, Vishwajeeth Pagala, Anna Stephan, Zane Coleman, Maricela Robles-Murguia, Yong-Dong Wang, Junmin Peng, and Fabio Demontis

Supplemental Figures

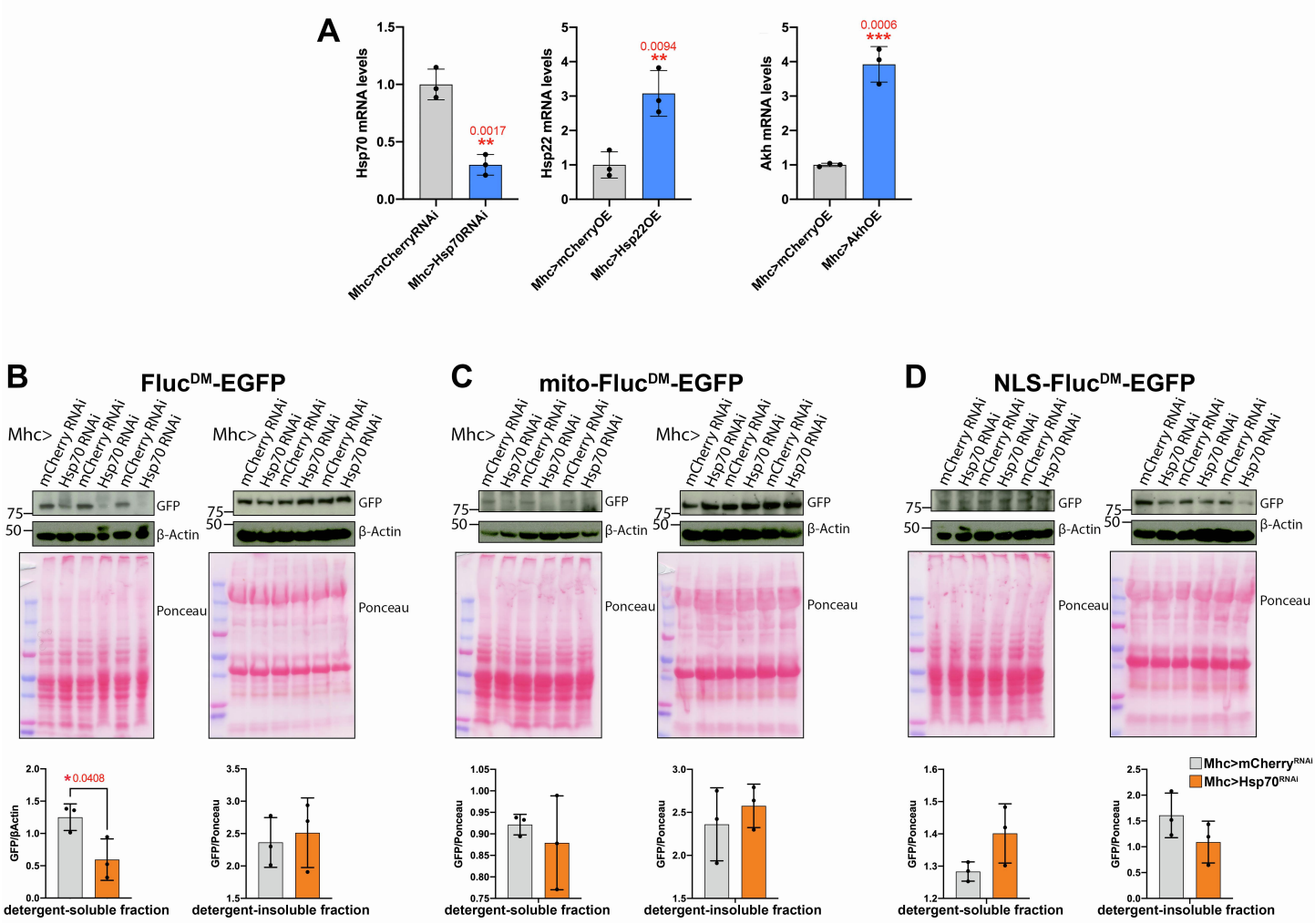

Figure S1. Hsp70 knockdown reduces the detergent-soluble levels of cytoplasmic Fluc^{DM}, related to Fig. 4.

(A) qRT-PCR validation of transgene expression. As expected, *Hsp70* mRNA levels decrease in response to Hsp70 RNAi in skeletal muscle whereas *Hsp22* mRNA levels increase in response to *Hsp22* overexpression. *Akh* mRNA levels increase upon *Akh* overexpression. In (A-B), n=3 (biological replicates) with the mean ±SD indicated; ***P*<0.01, ****P*<0.001 (unpaired two-tailed t-test).

(B-D) Western blots of detergent-soluble and insoluble fractions from skeletal muscle with Hsp70 knockdown (*Mhc>Hsp70^{RNAi}*; orange) versus controls (*Mhc>mCherry^{RNAi}*; gray). Anti-GFP antibodies were used to detect the EGFP-tagged Fluc^{DM} variants targeted to the cytoplasm (Fluc^{DM}; (B)), the mitochondria (mito-Fluc^{DM}; (C)), and the nucleus (NLS-Fluc^{DM}; (D)). Ponceau staining and β-actin are shown as normalization control. Hsp70 RNAi significantly decreases the detergent-soluble levels of the untargeted (~cytoplasmic) Fluc^{DM} whereas NLS-Fluc^{DM} and mito-Fluc^{DM} are not affected. N=3 (biological replicates) with the mean ±SD indicated; **P*<0.05 (unpaired two-tailed t-test).

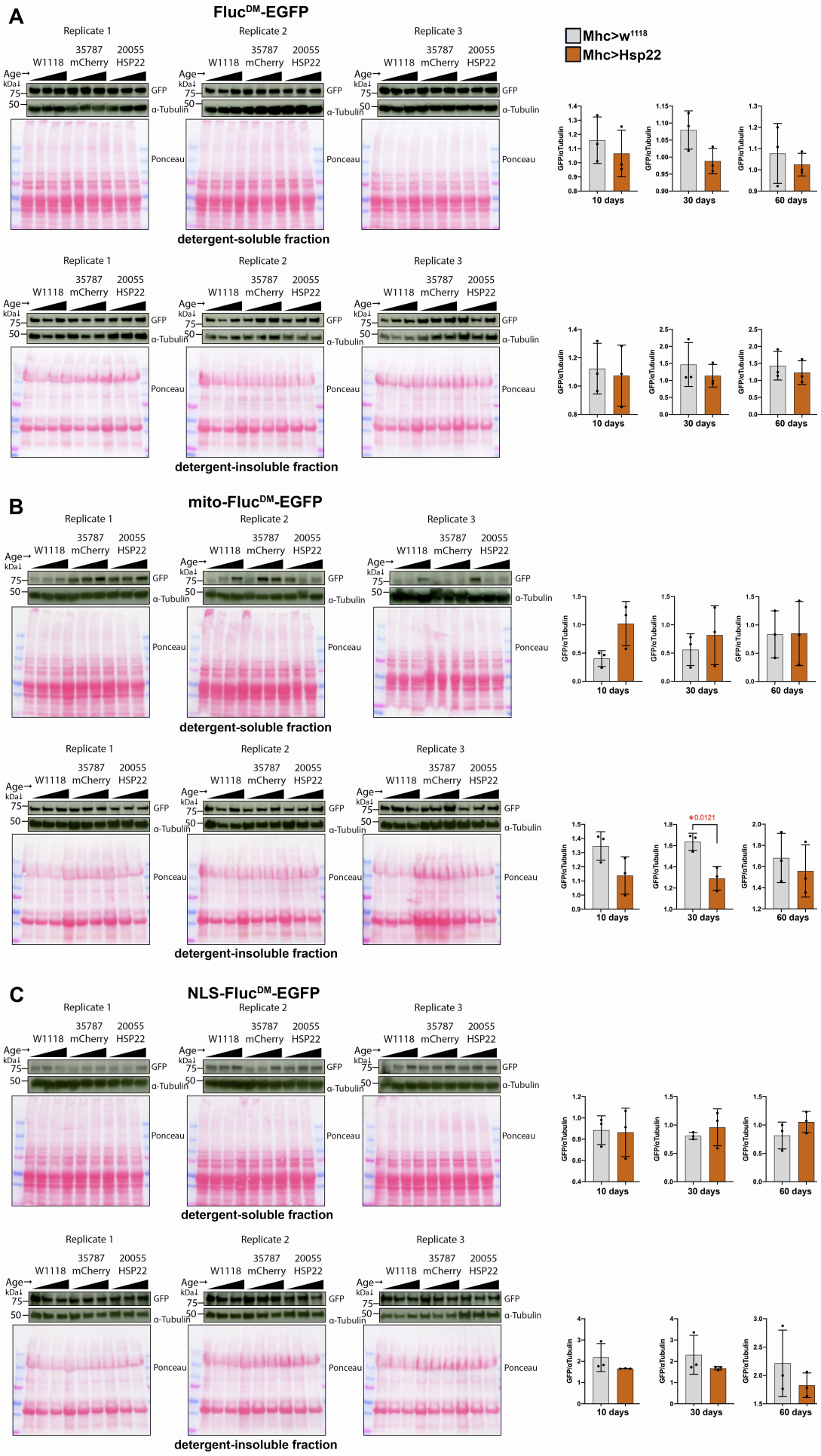
A
Fluc^DM-EGFP
Replicate 1
Replicate 2
Replicate 3
W1118
35787 mCherry
20055 HSP22
Age→
kDa↓
75
50
GFP
α-Tubulin
Ponceau
detergent-soluble fraction
detergent-insoluble fraction
Mhc>w1118
Mhc>Hsp22
GFP/αTubulin
10 days
30 days
60 days
B
mito-Fluc^DM-EGFP
C
NLS-Fluc^DM-EGFP
*0.0121

Figure S2. Hsp22 overexpression reduces the detergent-insoluble levels of mitochondrial Fluc^{DM}, related to Fig. 4.

(A-C) Western blots of detergent-soluble and insoluble fractions from skeletal muscle with Hsp22 overexpression (*Mhc>Hsp22*; brown) versus controls (*Mhc>w^{1118}*; gray). Anti-GFP antibodies were used to detect the EGFP-tagged Fluc^{DM} variants targeted to the cytoplasm (Fluc^{DM}; (A)), the mitochondria (mito-Fluc^{DM}; (B)), and the nucleus (NLS-Fluc^{DM}; (C)). Ponceau staining and α-tubulin are shown as normalization control. Hsp22 overexpression decreases the detergent-insoluble levels of mito-Fluc^{DM} (B). N=3 (biological replicates) with the mean ±SD; *P<0.05 (unpaired two-tailed t-test).

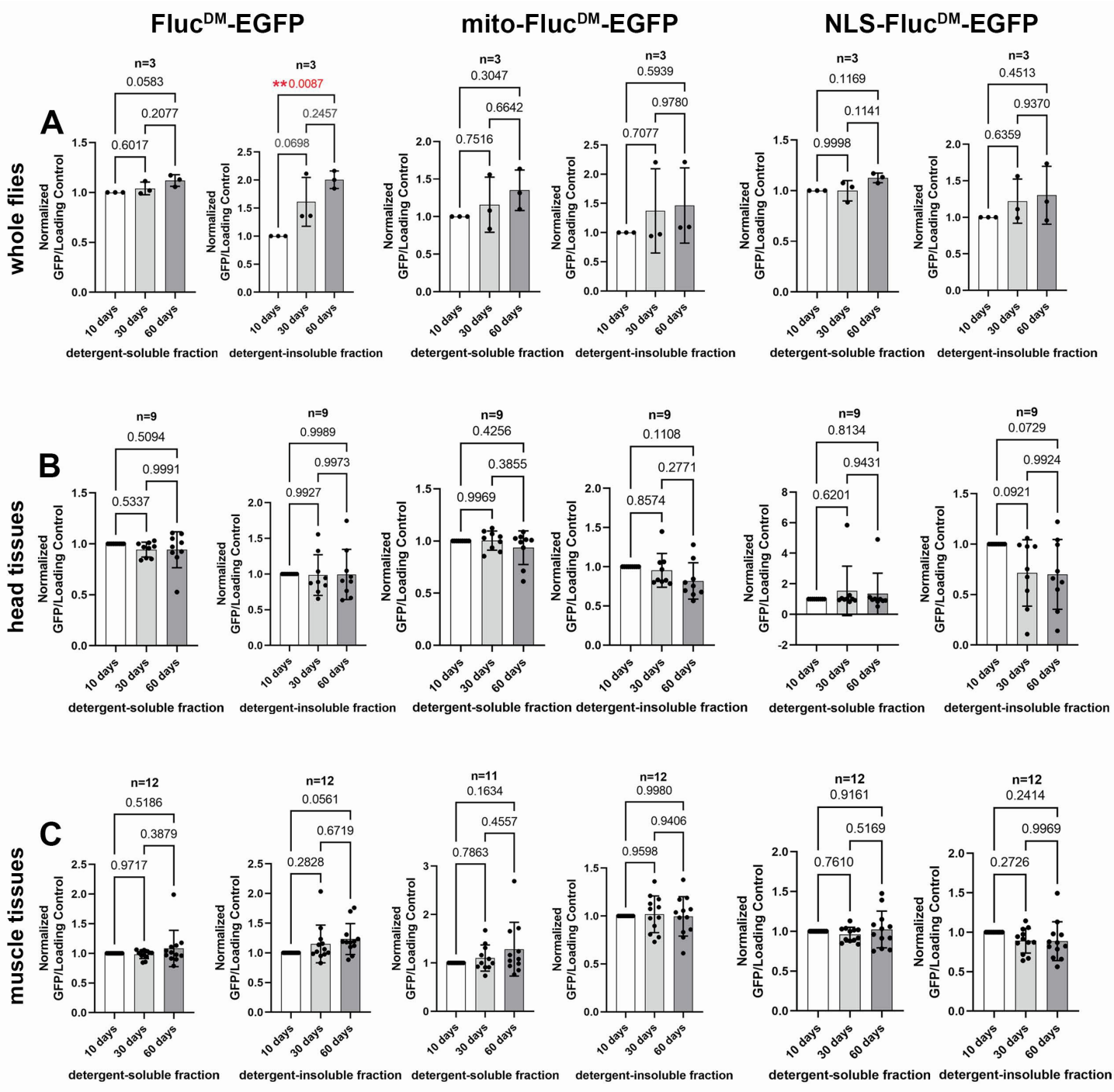

Figure S3. The solubility of Fluc^{DM} sensors is overall maintained during normal aging in *Drosophila*, related to Fig. 4.

(A-C) Western blots of detergent-soluble and insoluble fractions from whole flies (A), heads (B), and thoraces (C) at different ages (10, 30, and 60 days of age). There is a significant increase in the detergent-insoluble levels of Fluc^{DM} (but not of mito-Fluc^{DM} and NLS-Fluc^{DM}) with aging in extracts from whole flies. However, there is no modulation of the detergent-soluble and insoluble-levels of Fluc^{DM}, mito-Fluc^{DM}, and NLS-Fluc^{DM} in heads and thoraces, which are enriched respectively for tissues of the central nervous system and skeletal muscle. The n(biological replicates) is indicated in each figure, with the mean ±SD; $^{**}P<0.01$ (one-way ANOVA).

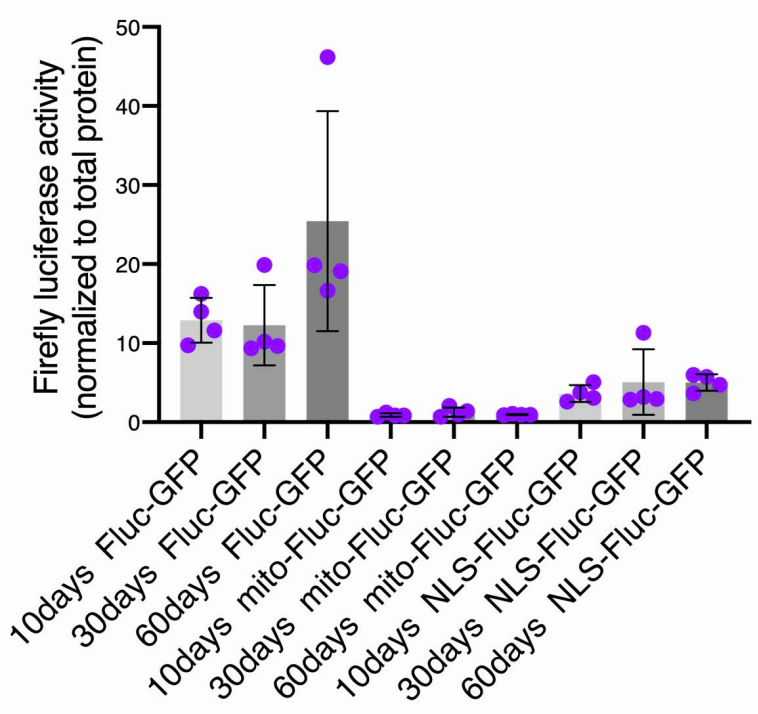

Figure S4. Monitoring the folding and activity of compartment-targeted Fluc^{DM} variants with luciferase assays, related to Fig. 4. Firefly luciferase assays from thoraces of flies with Fluc^{DM}-GFP, mito-Fluc^{DM}-GFP, and NLS-Fluc^{DM}-GFP at different ages (10, 30, and 60 days). The luminescence is normalized by the total protein content. There is no significant age-associated change in the luciferase activity of each Fluc^{DM} sensor in skeletal muscle (thoraces), consistent with the western blot results in Fig. S3C. The mean ±SD is shown with n=4.

The activity of the mitochondrial and nuclear luciferases (mito-Fluc^{DM}-GFP and NLS-Fluc^{DM}-GFP) is lower than that of the general, ~cytoplasmic Fluc^{DM}-GFP luciferase, presumably because the nuclear and mitochondrial luciferases are less active or less stable than the general Fluc^{DM} due to compartment-specific challenges to their activity and/or stability.

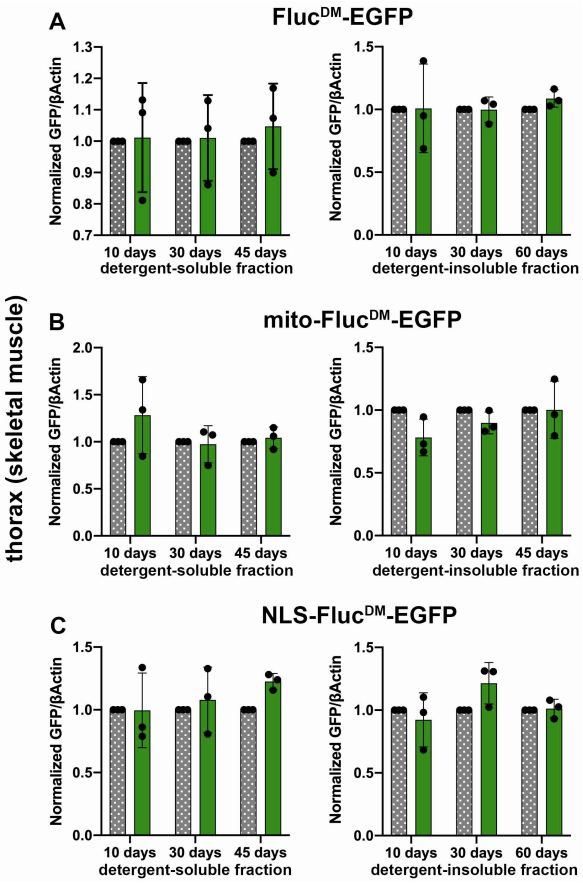

Figure S5. Amyrel does not regulate Fluc^{DM} solubility in skeletal muscle during aging, related to Fig. 5. (A-C) Quantification of normalized GFP/β-actin levels from western blots of thoracic extracts indicates that Amyrel (green) does not regulate proteostasis in skeletal muscles when compared to controls (gray).

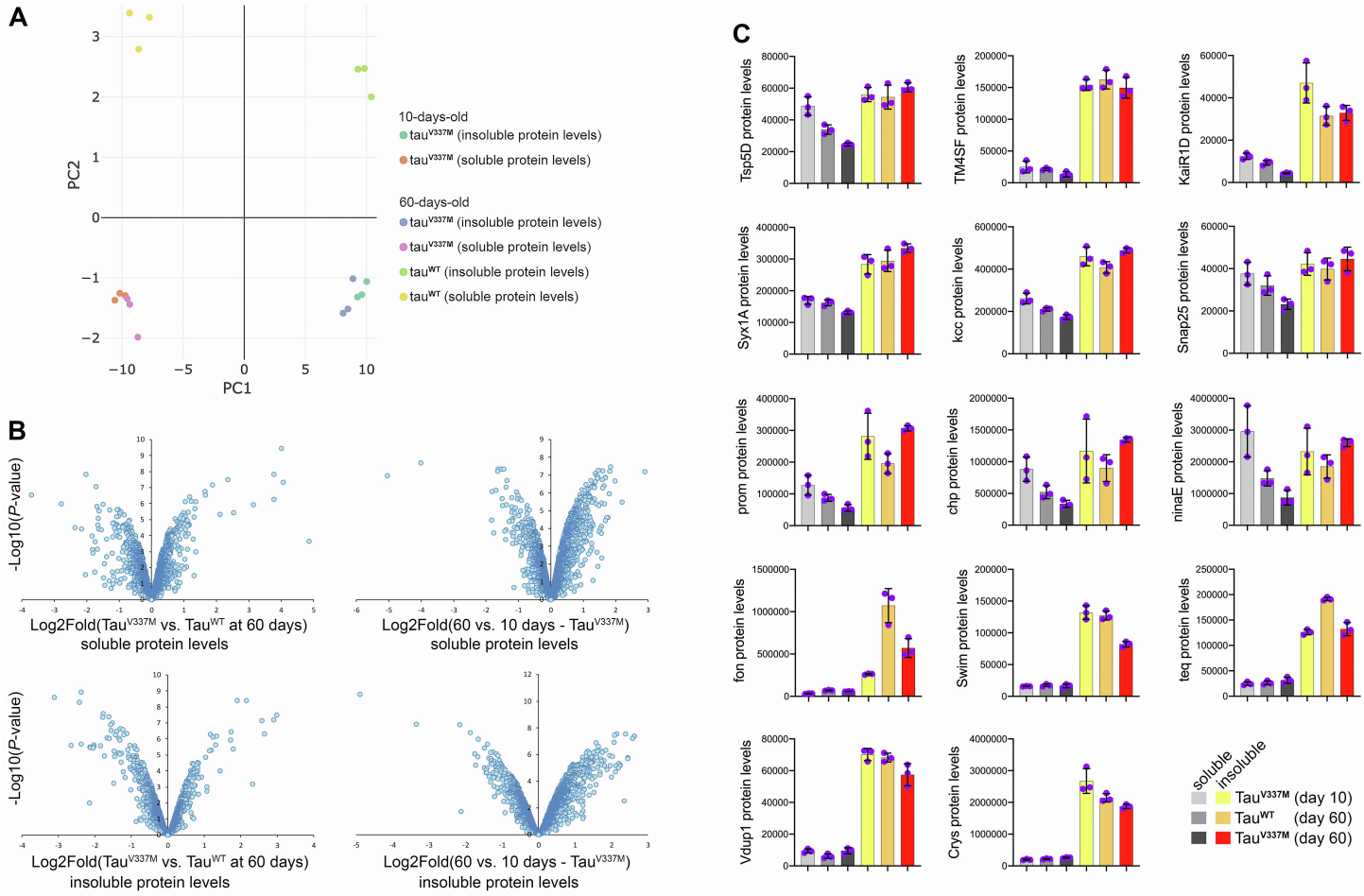

Figure S6. Changes in protein solubility induced by pathogenic tau^{V337M}, tau^{WT}, and aging in *Drosophila*, related to Fig. 7. (A) PCA of proteomics of detergent-soluble and insoluble fractions. (B) Overall representation of the proteomic changes induced by tau in detergent-soluble and insoluble fractions. The *y*-axis reports the -log$_{10}$(*P*-value) whereas the *x*-axis displays the log$_2$Fold changes induced by tau^{V337M} versus tau^{WT} in old age (left panels), and by tau^{V337M} at ~60 days versus 10 days (right panels) for the soluble (top panels) and insoluble (bottom panels) protein levels. (C) Graphs of detergent-soluble and insoluble levels of selected proteins with tau^{V337M}-induced changes in solubility. These graphs refer to the examples shown in Fig. 7H-I and report the detergent-soluble and insoluble levels of significantly regulated proteins (all *P*<0.05). N=3 (biological replicates) with the mean ±SD indicated.

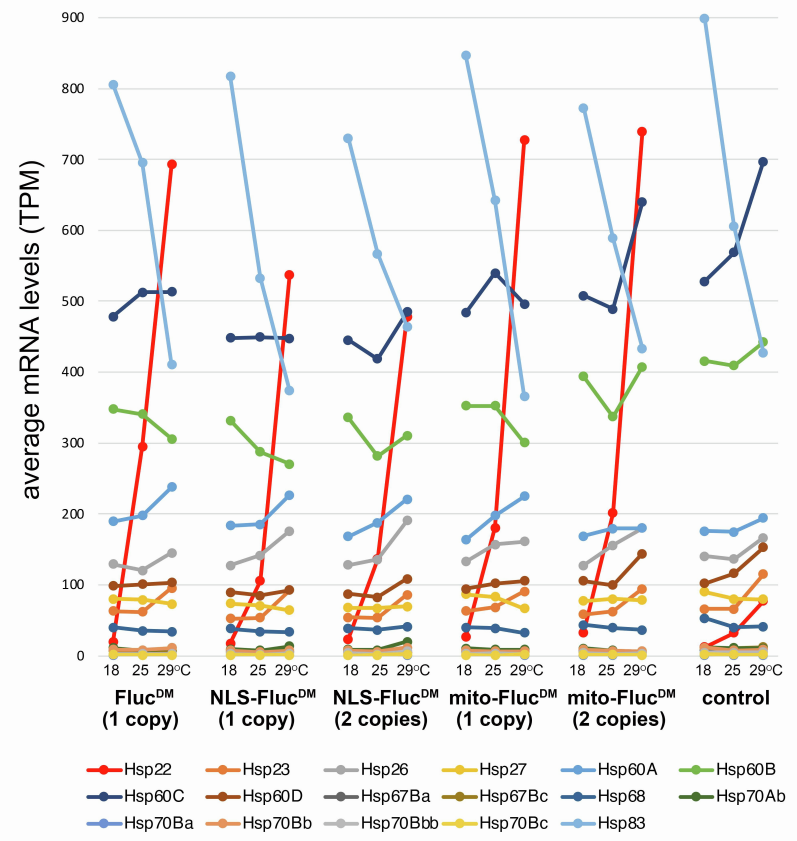

Figure S7. Fluc^{DM} proteins do not induce a heat shock response, related to Fig. 3. The average mRNA levels (TPM) of heat shock proteins were obtained from 3 biological replicates (Table S1). Compartment-targeted Fluc^{DM} variants do not have a major impact on the expression of heat shock proteins, compared to controls with no Fluc^{DM} expression. However, all Fluc^{DM} variants strongly induce the mitochondrial chaperone Hsp22 (red): this occurs at 18ºC and even more noticeably at 25ºC and 29ºC. Similar changes are induced by 1 versus 2 copies of the Fluc^{DM} transgenes. Apart from Hsp22, Fluc^{DM} variants do not appear to induce a heat shock-like response as they do not upregulate the expression of multiple chaperones but only of Hsp22.